Bioorganic & Medicinal Chemistry Letters 21 (2011) 4193–4196

Contents lists available at ScienceDirect

Bioorganic & Medicinal Chemistry Letters

journal homepage: www.elsevier.com/locate/bmcl

Novel quinoxaline derivatives for in vivo imaging of β-amyloid plaques in the brain

Mengchao Cui [a,b], Masahiro Ono [a,*], Hiroyuki Kimura [a], Boli Liu [b], Hideo Saji [a,*]

[a] Graduate School of Pharmaceutical Sciences, Kyoto University, 46-29 Yoshida Shimoadachi-cho, Sakyo-ku, Kyoto 606-8501, Japan
[b] Key Laboratory of Radiopharmaceuticals, Ministry of Education, College of Chemistry, Beijing Normal University, Beijing 100875, PR China

ARTICLE INFO

Article history:
Received 17 March 2011
Revised 20 May 2011
Accepted 23 May 2011
Available online 27 May 2011

Keywords:
Alzheimer's disease
β-Amyloid
Imaging agent
Binding assay
Autoradiography

ABSTRACT

In a search for new probes to detect β-amyloid plaques in the brain of patients with Alzheimer's disease (AD), we have synthesized and evaluated a series of quinoxaline derivatives containing a '6+6–6' ring system. These quinoxaline derivatives showed excellent affinity for $A\beta_{1-42}$ aggregates with K_i values ranging from 2.6 to 10.7 nM. Autoradiography with sections of brain tissue from an animal model of AD mice (APP/PS1) and AD patients revealed that [^{125}I]**5** labeled β-amyloid plaques specifically. In biodistribution experiments using normal mice, [^{125}I]**5** displayed high uptake (6.03% ID/g at 2 min) into and a moderately fast washout from the brain. Although additional refinements are needed to decrease the lipophilicity and improve the washout rate, the quinoxaline scaffold may be useful as a backbone structure to develop novel β-amyloid imaging agents.

Alzheimer's disease (AD) is the most common form of dementia in older people, and is estimated to account for 50% to 70% of dementia cases. Senile plaques containing β-amyloid (Aβ) aggregates and neurofibrillary tangles composed of highly phosphorylated tau protein are the two key pathological findings in postmortem AD brains.[1,2] The precise molecular mechanisms leading to the development of this disease are not fully understood, however, the amyloid cascade hypothesis is the most accepted explanation for the pathogenesis of AD.[3]

With modern functional neuroimaging techniques such as positron emission tomography (PET) and single photon emission tomography (SPECT), radio-labeled probes that specifically target Aβ plaques may aid in the diagnosis and monitoring of AD in living subjects. Thus, many efforts have focused on developing radiotracers or agents that allow Aβ imaging in vivo. An uncharged Thioflavin T (ThT) analogue, [^{11}C]PIB (2-(4′-[^{11}C]methylaminophenyl)-6-hydroxybenzothiazole), which is highly efficient both in crossing the blood–brain barrier (BBB) and in selective binding to Aβ plaques, is the most widely used amyloid marker with PET for amyloid imaging.[4,5] Recently, a close analogue of PIB, [^{11}C]AZD2184 ([^{11}C]-2-[6-(methylamino)pyridin-3-yl]-1,3-benzothiazol-6-ol), with a high affinity for Aβ fibrils in vitro was reported. Preliminary PET studies indicated that this probe displayed fast kinetics and an excellent contrast for Aβ plaques in the brain of AD patients.[6,7] Compared with ^{11}C ($t_{1/2}$: 20 min), ^{18}F with a longer half-life ($t_{1/2}$: 110 min) would be more useful for routine clinical use. In fact, a ^{18}F-labeled PIB analogue, [^{18}F]GE-067 ([^{18}F]-2-(3-fluoro-4-(methylamino)phenyl)benzo[d]thiazol-6-ol)[8], and two stilbene derivatives with fluorinated polyethylene glycol (PEG) units, [^{18}F]BAY94-9172 ([^{18}F]-4-(*N*-methylamino)-4′-(2-(2-(2-fluoroethoxy)ethoxy)ethoxy)-stilbene)[9] and [^{18}F]AV-45 ([^{18}F]-(*E*)-4-(2-(6-(2-(2-(2-fluoroethoxy)ethoxy)ethoxy)pyridin-3-yl)vinyl)-*N*-methylaniline)[10], are currently under phase II or phase III clinical trials. However, since the failure of [^{123}I]IMPY ([^{123}I]-6-iodo-2-(4′-dimethylamino-)phenyl-imidazo[1,2]pyridine) in clinical trials, there has been no report of any Aβ imaging agents for SPECT moving into clinical testing.[11–13]

Most of these Aβ probes were derived from the basic structure of thioflavin-T, which consists of a six-membered ring fused to a

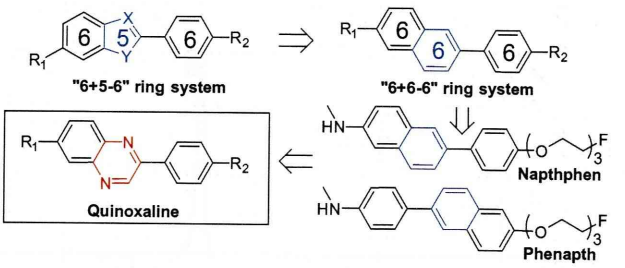

Figure 1. Design strategy for the quinoxaline derivatives as probes for Aβ plaques.

* Corresponding authors. Tel.: +81 75 753 4608; fax: +81 75 753 4568 (M.O.); tel.: +81 75 753 4556; fax: +81 75 753 4568 (H.S.).
E-mail addresses: ono@pharm.kyoto-u.ac.jp (M. Ono), hsaji@pharm.kyoto-u.ac.jp (H. Saji).

0960-894X/$ - see front matter © 2011 Elsevier Ltd. All rights reserved.
doi:10.1016/j.bmcl.2011.05.079

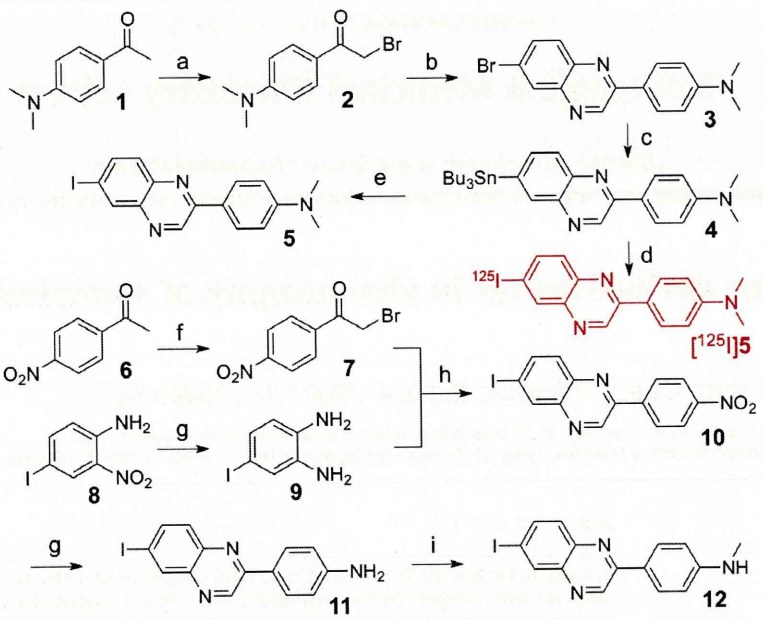

Scheme 1. Reagents and conditions: (a) 1: conc. H_2SO_4, Br_2, 0 °C to rt 2: ethyl phosphite, Et_3N, THF, 0 °C to rt; (b) 4-bromobenzene-1,2-diamine, DMSO, rt; (c) $(Bu_3Sn)_2$, $(PPh_3)_4Pd$, dioxane, Et_3N, reflux; (d) [^{125}I]NaI, HCl (1 M), H_2O_2 (3%), rt; (e) I_2, $CHCl_3$, rt; (f) Br_2, Et_2O, 0 °C to rt; (g) $SnCl_2$, EtOH, conc. HCl, reflux; (h) DMSO, rt; (i) acetone, CH_3I, K_2CO_3.

five-membered heterocyclic ring together with another conjugated six-membered ring, creating a '6+5–6' ring system (Fig. 1). In an attempt to further develop novel ligands for the imaging of amyloid plaques through enlargement of the five-membered ring, Zhang et al. reported two fluoro-pegylated phenapth or napthphen derivatives as PET probes which contain a '6+6–6' ring system.[14] However, the naphthalene ring is highly lipophilic which may cause high non-specific binding. To reduce the lipophilicity, we have selected quinoxaline instead of the naphthalene ring. Herein, we report the synthesis and biological evaluation of quinoxaline derivatives as potential Aβ imaging agents.

The synthesis of quinoxaline derivatives is described in Scheme 1, starting from α-bromoacetophenone and substituted

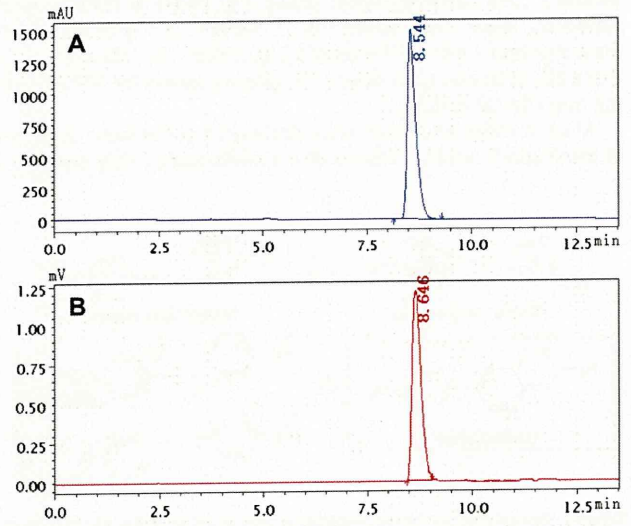

Figure 2. HPLC profiles of **5** (A) and [^{125}I]**5** (B). HPLC conditions: Cosmosil C18 column (Nakalai Tesque, 5C_{18}-AR-II, 4.6 mm × 150 mm), CH_3CN/H_2O = 90/10, 1 mL/min, UV, 254 nm, **5** t_R (UV) = 8.54 min, [^{125}I]**5** t_R (RI) = 8.65 min.

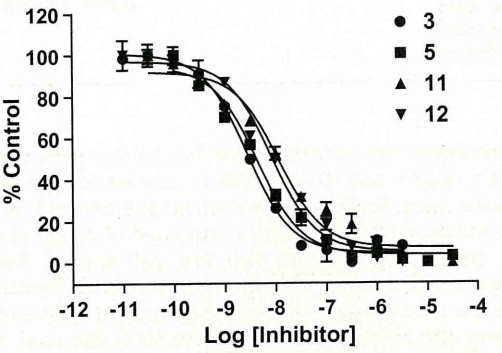

Figure 3. Inhibition curves for the binding of [^{125}I]IMPY to Aβ_{1-42} aggregates.

o-phenylenediamines. The intermediates α-bromoacetophenone (**2** and **7**) and 4-iodobenzene-1,2-diamine (**9**) were prepared first based on procedures reported previously.[15] In the presence of DMSO, the quinoxaline backbone was formed by an one-pot tandem oxide condensation procedure in moderate yields (**3**: 36.7%, **10**: 49.1%). Two isomeric products were obtained depending on the course of cyclization, the corresponding 2-aryl-6-substituted quinoxalines (**3** and **10**) as major products and the 2-aryl-7-substituted quinoxalines as minor products. Furthermore, the crystal structure of **3** was determined by X-ray crystallography (see Supplementary data). The free amino derivative **11** was achieved by reducing a nitro group to an amino group with $SnCl_2$ in ethanol under reflux condition (87.0%). Conversion of **11** to the *N*-methylamino derivative **12** was achieved by methylation with CH_3I under alkaline conditions. The desired tributyltin precursor **4** was prepared by $Pd(PPh_3)_4$-catalyzed *trans*-stannylation from the bromide compound **3** (31.5%). The subsequent iododestannylation reaction afforded the iodinated target **5** (21.8%).

The desired radioiodinated ligand [^{125}I]**5** was successfully prepared from the corresponding tributyltin precursors through

Table 1
Inhibition constants (K_i, nM) for the binding of [^{125}I]IMPY to $A\beta_{1-42}$ aggregates.

Compound	R_1	R_2	K_i (nM)[a]
3	Br	$N(CH_3)_2$	2.6 ± 0.2
5	I	$N(CH_3)_2$	4.1 ± 0.7
11	I	NH_2	10.7 ± 1.1
12	I	$NHCH_3$	7.7 ± 1.4
IMPY	–	–	10.5 ± 1.0

[a] Values are the mean for three independent experiments.

standard iododestannylaltion reactions, using sodium [^{125}I]iodide, hydrogen peroxide, and hydrochloric acid (Scheme 1). The overall radiochemical yield for [^{125}I]**5** was 62.3%. The radiochemical identity of the ^{125}I-labeled ligands was confirmed by co-injection with nonradioactive compounds from HPLC profiles (Fig. 2). The purified ligands all had a radiochemical puritiy greater than 98% and high specific activity (no carrier added, approx. 81.4 TBq/mmol).

The affinity (K_i, nM) of the quinoxaline compounds was evaluated based on inhibition of the binding of [^{125}I]IMPY to aggregates of $A\beta_{1-42}$ fibers in solution (Fig. 3). The results are presented in Table 1. All of the compounds showed excellent affinity for Aβ aggregates ($K_i \leqslant 10$ nM). The results indicated that these quinoxaline derivatives bind to the same site as [^{125}I]IMPY. From the K_i values listed in Table 1, it is clear that the tertiary *N,N*-dimethylamino analogues **3** and **5** have higher affinity (K_i = 2.6 and 4.1 nM, respectively) than the secondary *N*-methylamino analogue **12** (K_i = 7.7 nM), while the corresponding primary amino analogue **11** showed moderate affinity (K_i = 10.7 nM), which is consistent with previous data on primary, secondary, and tertiary amino ligands.[16] The K_i values of these quinoxaline derivatives are similar to that of phenapth or napthphen derivatives (K_i = 1.6 nM and 3.0 nM) reported previously.[14] Due to the encouraging binding data for these quinoxaline compounds, the tertiary *N,N*-dimethylamino analogue (**5**) was selected for radiolabeling and further biological evaluation.

To confirm the specific binding of **5** to Aβ plaques, the fluorescent staining of sections of brain tissue from an animal model of AD (C57BL6, APP/PS1 mouse, 12 months) was performed. As shown in Figs. 4, 5 clearly labeled Aβ plaques with low background levels (Fig. 4A), the labeling pattern consistent with that obtained on staining with thioflavin-S in adjacent sections (Fig. 4B).

Next, in vitro autoradiography was carried out in brain sections of AD patients and double transgenic mice using the radioiodinated

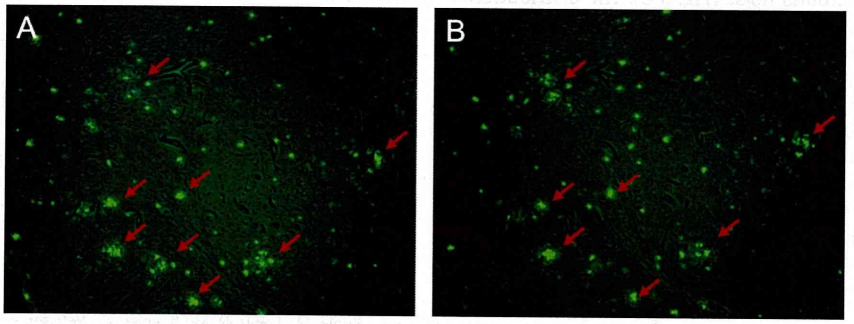

Figure 4. Fluorescence staining of **5** (A) in a section of brain tissue from a Tg model mouse (C57BL6, APP/PS1, 12 months old, male) with a filter set for GFP. The presence of plaques was confirmed by staining of the adjacent section with thioflavin S (B).

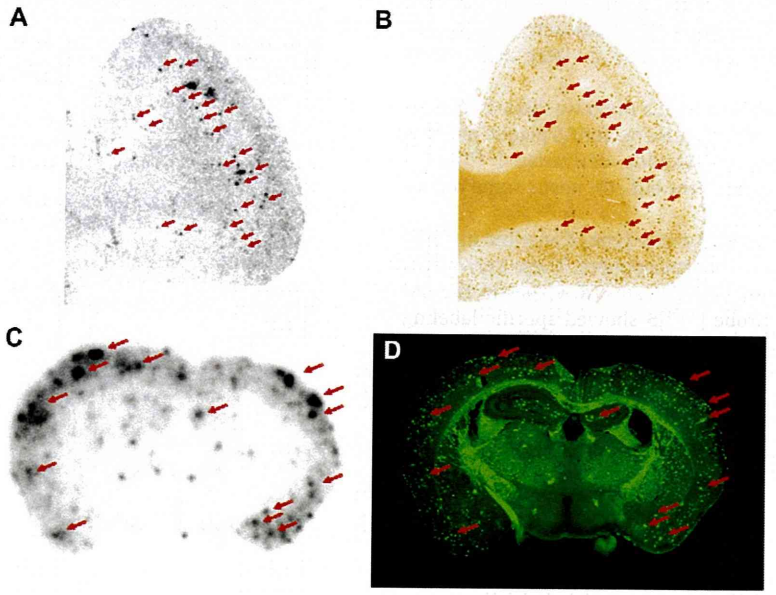

Figure 5. Autoradiography of [^{125}I]**5** in vitro in brain sections of an AD patient (A) and Tg mouse (C57BL6, APP/PS1, 12 months old, male) (C). The presence and distribution of plaques in the sections were confirmed with immunohistochemical staining using a monoclonal Aβ antibody (B) and thioflavin-S (D). Arrows show the correspondence to Aβ plaques.

Table 2
Biodistribution in normal ddy mice after iv injection of [^{125}I]**5**[a] and the lipophilicity (log *D*) of the ligand

[^{125}I]**5** Log *D* = 4.02 ± 0.12				
Organ	2 min	30 min	60 min	120 min
Blood	4.71 ± 1.04	2.88 ± 0.62	2.98 ± 1.04	1.88 ± 0.55
Brain	6.03 ± 0.99	5.21 ± 1.16	2.91 ± 1.18	1.12 ± 0.31
Heart	14.91 ± 2.11	2.53 ± 0.77	2.17 ± 0.69	1.22 ± 0.29
Liver	30.49 ± 7.74	15.73 ± 3.76	12.50 ± 5.00	7.53 ± 2.51
Spleen	5.69 ± 1.79	2.82 ± 0.76	2.22 ± 0.86	1.17 ± 0.23
Lung	14.53 ± 5.53	3.99 ± 1.08	3.53 ± 1.27	1.95 ± 0.42
Kidney	19.67 ± 4.99	8.76 ± 2.72	6.68 ± 2.53	3.96 ± 0.96
Stomach[b]	2.06 ± 0.39	3.28 ± 0.72	5.39 ± 1.66	8.62 ± 2.40
Intestine	3.43 ± 0.83	18.62 ± 12.17	22.50 ± 9.17	16.93 ± 5.92

[a] Expressed as % injected dose per gram. Average for five mice ± standard deviation.
[b] Expressed as % injected dose per organ.

ligand [^{125}I]**5**. As shown in Figure 5A, specific labeling of plaques was observed in AD brains. Immunohistochemical staining confirmed the presence of plaques in these sections (Fig. 5B). As expected, [^{125}I]**5** also labeled Aβ plaques in the brain sections of transgenic mice, with numerous fluorescent spots in the cortex region, and minimal background noise (Fig. 5 C). The distribution of Aβ plaques was consistent with the results of autoradiography with thioflavin-S (Fig. 5D).

Although two nitrogen atoms were introduced into the aromatic system of the quinoxaline structure, a high log *D* value (4.02) for [^{125}I]**5** was obtained under the experimental conditions, a reflection of the lipophilic properties of the radioiodinated ligand. Nonetheless, biodistribution experiments in normal mice (Table 2) clearly indicated that [^{125}I]**5** readily penetrated the intact BBB showing excellent initial uptakes into the brain (6.03 ± 0.99% ID/g) at 2 min after injection. Since there are no Aβ plaques in normal mice, the high uptake was subsequently followed by a moderate washout with 1.12% ID/g at 120 min. Compared with the fluoropegylated phenapth derivatives (3.80)[14], the radioiodinated ligand [^{125}I]**5** in this study had superior $\text{brain}_{2\ \text{min}}/\text{brain}_{120\ \text{min}}$ ratios (5.38). In addition, the blood background level during the experiment was lower than the brain uptake, which is good for reducing nonspecific binding. [^{125}I]**5** was excreted predominantly by the hepatobiliary and excretory systems, and radioactivity was observed to accumulate within the intestine at later time points (16.93% ID/g at 120 min).

A good initial uptake combined with a rapid washout from normal brain tissue are important requirements for Aβ plaque imaging agents.[17] The radioiodinated quinoxaline derivative [^{125}I]**5** reported here, met the first requirement but still needs some refinements to improve its washout rate.

In summary, we have developed a new type of amyloid imaging agent based on the quinoxaline pharmacophore. These derivatives displayed high affinity for $A\beta_{1-42}$ aggregates (K_i values in the nM range). The radioiodinated probe [^{125}I]**5** showed specific labeling of Aβ plaques in sections of brain tissue from AD patients and transgenic mice. In addition, [^{125}I]**5** readily enters the brain and was washed out from the normal mouse brain moderately quickly. Further refinements are under way to decrease the lipophilicity of this probe and improve its rate of washout from the brain. These quinoxaline ligands could be potentially useful for the imaging of Aβ plaques in living subjects.

Acknowledgements

This study was supported by the Japan Society for the Promotion of Science (JSPS) through the "Funding Program for Next Generation World-Leading Researchers (NEXT Program)" initiated by the Council for Science and Technology Policy (CSTP), and a Grant-in-aid for Young Scientists (A) and Exploratory Research from the Ministry of Education, Culture, Sports, Science and Technology, Japan. This study was also supported by the China Scholarship Council (CSC).

Supplementary data

Supplementary data associated with this article can be found, in the online version, at doi:10.1016/j.bmcl.2011.05.079.

References and notes

1. Hardy, J. A.; Higgins, G. A. *Science* **1992**, *256*, 184.
2. Selkoe, D. J. *JAMA-J. Am. Med. Assoc.* **2000**, *283*, 1615.
3. Hardy, J. A.; Selkoe, D. J. *Science* **2002**, *297*, 353.
4. Mathis, C. A.; Wang, Y.; Holt, D. P.; Huang, G. F.; Debnath, M. L.; Klunk, W. E. *J. Med. Chem.* **2003**, *46*, 2740.
5. Klunk, W. E.; Engler, H.; Nordberg, A.; Wang, Y.; Blomqvist, G.; Holt, D. P.; Bergstrom, M.; Savitcheva, I.; Huang, G. F.; Estrada, S.; Ausen, B.; Debnath, M. L.; Barletta, J.; Price, J. C.; Sandell, J.; Lopresti, B. J.; Wall, A.; Koivisto, P.; Antoni, G.; Mathis, C. A.; Langstrom, B. *Ann. Neurol.* **2004**, *55*, 306.
6. Andersson, J. D.; Varnas, K.; Cselenyi, Z.; Gulyas, B.; Wensbo, D.; Finnema, S. J.; Swahn, B. M.; Svensson, S.; Nyberg, S.; Farde, L.; Halldin, C. *Synapse* **2010**, *64*, 733.
7. Nyberg, S.; Jonhagen, M. E.; Cselenyi, Z.; Halldin, C.; Julin, P.; Olsson, H.; Freund-Levi, Y.; Andersson, J.; Varnas, K.; Svensson, S.; Farde, L. *Eur. J. Nucl. Med. Mol. Imaging* **2009**, *36*, 1859.
8. Koole, M.; Lewis, D. M.; Buckley, C.; Nelissen, N.; Vandenbulcke, M.; Brooks, D. J.; Vandenberghe, R.; Van Laere, K. *J. Nucl. Med.* **2009**, *50*, 818.
9. Rowe, C. C.; Ackerman, U.; Browne, W.; Mulligan, R.; Pike, K. L.; O'Keefe, G.; Tochon-Danguy, H.; Chan, G.; Berlangieri, S. U.; Jones, G.; Dickinson-Rowe, K. L.; Kung, H. F.; Zhang, W.; Kung, M. P.; Skovronsky, D.; Dyrks, T.; Holl, G.; Krause, S.; Friebe, M.; Lehman, L.; Lindemann, S.; Dinkelborg, L. M.; Masters, C. L.; Villemagne, V. L. *Lancet Neurol.* **2008**, *7*, 129.
10. Choi, S. R.; Golding, G.; Zhuang, Z. P.; Zhang, W.; Lim, N.; Hefti, F.; Benedum, T. E.; Kilbourn, M. R.; Skovronsky, D.; Kung, H. F. *J. Nucl. Med.* **2009**, *50*, 1887.
11. Kung, M. P.; Hou, C.; Zhuang, Z. P.; Zhang, B.; Skovronsky, D.; Trojanowski, J. Q.; Lee, V. M.; Kung, H. F. *Brain Res.* **2002**, *956*, 202.
12. Zhuang, Z. P.; Kung, M. P.; Wilson, A.; Lee, C. W.; Plossl, K.; Hou, C.; Holtzman, D. M.; Kung, H. F. *J. Med. Chem.* **2003**, *46*, 237.
13. Newberg, A. B.; Wintering, N. A.; Plossl, K.; Hochold, J.; Stabin, M. G.; Watson, M.; Skovronsky, D.; Clark, C. M.; Kung, M. P.; Kung, H. F. *J. Nucl. Med.* **2006**, *47*, 748.
14. Zhang, W.; Kung, M.-P.; Hou, C.; Oya, S.; Skovronsky, D.; Manchanda, R.; Choi, S.-R.; Kung, H. *J. Nucl. Med.* **2008**, *49*, 143P.
15. Hindo, S. S.; Mancino, A. M.; Braymer, J. J.; Liu, Y.; Vivekanandan, S.; Ramamoorthy, A.; Lim, M. H. *J. Am. Chem. Soc.* **2009**, *131*, 16663.
16. Cai, L. S.; Innis, R. B.; Pike, V. W. *Curr. Med. Chem.* **2007**, *14*, 19.
17. Kung, H. F.; Choi, S. R.; Qu, W. C.; Zhang, W.; Skovronsky, D. *J. Med. Chem.* **2010**, *53*, 933.

Bioorganic & Medicinal Chemistry 19 (2011) 4148–4153

Contents lists available at ScienceDirect

Bioorganic & Medicinal Chemistry

journal homepage: www.elsevier.com/locate/bmc

Synthesis and evaluation of benzofuran-2-yl(phenyl)methanone derivatives as ligands for β-amyloid plaques

Mengchao Cui [a,b], Masahiro Ono [a,*], Hiroyuki Kimura [a], Boli Liu [b], Hideo Saji [a,*]

[a] Graduate School of Pharmaceutical Sciences, Kyoto University, 46-29 Yoshida Shimoadachi-cho, Sakyo-ku, Kyoto 606-8501, Japan
[b] Key Laboratory of Radiopharmaceuticals, Ministry of Education, College of Chemistry, Beijing Normal University, Beijing 100875, PR China

ARTICLE INFO

Article history:
Received 3 March 2011
Revised 26 April 2011
Accepted 26 April 2011
Available online 3 May 2011

Keywords:
Alzheimer's disease
β-Amyloid
Imaging agent
Binding assay
Autoradiography

ABSTRACT

A series of benzofuran-2-yl(phenyl)methanone derivatives were synthesized and evaluated as novel probes for β-amyloid plaques. These derivatives were produced by a Rap–Stoermer condensation reaction. Compounds with a *N,N*-dimethylamino group displayed high affinity for $A\beta_{1-42}$ aggregates with K_i values in the nanomolar range. Autoradiography with brain sections of AD model mice (APP/PS1) revealed that a radioiodinated probe, [^{125}I]**10**, labeled β-amyloid plaques selectively and displayed good brain uptake (3.53% ID/g) at 2 min. The results suggest that benzofuran-2-yl(phenyl)methanone derivatives should be investigated further as potential probes for detecting β-amyloid plaques in the AD brain.

1. Introduction

Alzheimer's disease (AD) is a progressive brain disorder that causes problems with memory, thinking and behavior. Although the etiology of AD is not completely understood, β-amyloid (Aβ) plaques and neurofibrillary tangles (NFTs) found in the brain are the best known histological hallmarks of the disease.[1–3] A clinical diagnosis based on neurological examinations and clinical history is often difficult and unreliable, and a definite diagnosis can only be made by post-mortem investigation to detect Aβ plaques in brain tissue. However, noninvasive functional imaging techniques such as positron emission tomography (PET) and single photon emission computed tomography (SPECT) together with specific in vivo imaging agents targeting Aβ plaques would allow a more accurate diagnosis of AD.[4,5]

Over recent years, great efforts have been made to develop radiotracers that specifically bind to Aβ plaques in vivo (Fig. 1). [^{11}C]PIB (2-(4′-[11C]methylaminophenyl)-6-hydroxybenzothiazole), a neutral Thioflavin T (ThT) derivative widely used as a PET radioligand for amyloid imaging, clearly distinguishes between AD and control cases.[6,7] Currently, a fluorine-18-labeled PIB analogue, [^{18}F]GE-067 ([^{18}F]-2-(3-fluoro-4-(methylamino) phenyl)benzo[*d*]thiazol-6-ol),[8] and two stilbene derivatives with fluorinated polyethylene glycol (PEG) units, [^{18}F]BAY94-9172 ([^{18}F]-4-(*N*-methylamino)-4′-(2-(2-(2-fluoroethoxy)ethoxy)ethoxy)-stilbene)[9,10] and [^{18}F]AV-45 ([^{18}F]-(*E*)-4-(2-(6-(2-(2-(2-fluoroeth-

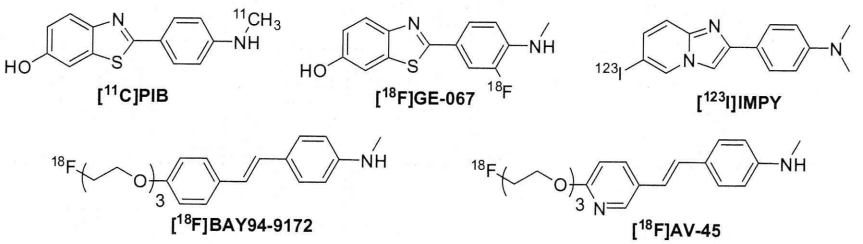

Figure 1. Chemical structure of Aβ imaging probes in clinical trials.

* Corresponding authors. Tel.: +81 75 753 4608; fax: +81 75 753 4568 (M.O.), tel.: +81 75 753 4556; fax: +81 75 753 4568 (H.S.).
E-mail addresses: ono@pharm.kyoto-u.ac.jp (M. Ono), hsaji@pharm.kyoto-u.ac.jp (H. Saji).

0968-0896/$ - see front matter © 2011 Elsevier Ltd. All rights reserved.
doi:10.1016/j.bmc.2011.04.049

oxy)ethoxy)ethoxy)pyridin-3-yl)vinyl)-*N*-methylaniline),[11–13] are being evaluated in phase II and phase III clinical trials. In addition, an iodine-123-labeled agent, [^{123}I]IMPY ([^{123} I]-6-iodo-2-(4′-dimethylamino-)phenyl-imidazo[1,2]pyridine) is the first SPECT probe to be evaluated in humans (Fig. 1).[14–16] However, a poor signal-to-noise ratio makes it difficult to distinguish AD patients.

In a search for novel Aβ imaging probes, we have found that chalcone derivatives displayed excellent affinity for Aβ aggregates, with some of them showing good uptake into and rapid clearance from the brain.[17–19] By selectively fixing the ketone part of the chalcone through an oxygen atom, we obtained a series of iodine-125-labeled aurone derivatives (Fig. 2), which showed high binding to Aβ aggregates.[20] Notably, the PEGylated aurone derivatives displayed improved pharmacokinetics in vivo, and may served as potential Aβ imaging probes for SPECT.[21] However, the conjugated double bonds in the chalcone and aurone structure may form cis–trans isomers. Herein, we report a series of benzofuran-2-yl(phenyl)methanone derivatives with a fixed double bond of chalcone as novel Aβ imaging agents (Fig. 2). This is the first time benzofuran-2-yl(phenyl)methanone derivatives have been proposed as Aβ imaging probes for detecting AD.

2. Results and discussion

2.1. Chemistry

The synthesis of benzofuran-2-yl(phenyl)methanone derivatives was readily accomplished by the reactions shown in Schemes 1 and 2. The α-bromination of 4-nitroacetophenone (**1**) with bromine in ethylether under room temperature afforded **2** in an excellent yield of 94%. Formation of the benzofuran-2-yl(phenyl)methanone backbone was achieved by a Rap–Stoermer condensation reaction between the substituted salicylaldehyde and α-haloacetophenone mediated by K_2CO_3 in acetone at room temperature. Compounds **3** and **4** were obtained in good chemical yields (84% and 87%, respectively). The free amino derivatives **5** and **6** were obtained by reducing a nitro group to an amino group with $SnCl_2$ in ethanol under reflux condition (90% and 81%, respectively). Conversion of the amino derivatives **5** and **6** to the *N*-methylamino or *N,N*-dimethylamino derivatives was achieved by methylation with CH_3I under alkaline conditions in one step. The desired tributyltin precursors **11** and **12** were prepared by $Pd(PPh_3)_4$-catalyzed trans-stannylation from their bromide compounds (18% and 29%, respectively).

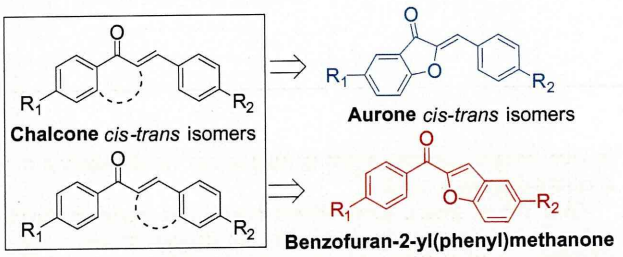

Figure 2. Design strategy of the benzofuran-2-yl(phenyl)methanone derivatives as probes for Aβ plaques.

2.2. Binding assay in vitro using $Aβ_{1–42}$ aggregates

The affinity (K_i, nM) of the newly synthesized benzofuran-2-yl(phenyl)methanone derivatives were first evaluated by in vitro competitive binding assays with [^{125}I]IMPY for aggregates of $Aβ_{1–42}$ fibers in solution.[15] IMPY and [^{125}I]IMPY were prepared based on previously reported procedures,[15] and IMPY was also screened under the same assay system for comparison. The derivatives inhibited the binding of [^{125}I]IMPY to $Aβ_{1–42}$ fibers in a dose-dependent manner, indicating an affinity for Aβ aggregates (Fig. 3). As shown in Table 1, the tertiary *N,N*-dimethylamino analogues **9** and **10** were found to have higher affinity (K_i = 8.8 and 6.6 nM, respectively) than the secondary *N*-methylamino analogues **7** and **8**, while the corresponding primary amino analogues **5** and **6** showed low affinity (K_i = 156.6 and 133.2 nM, respectively), which is consistent with previous data on primary, secondary, and tertiary amino ligands.[5] Compounds **3** and **4** containing an electron-withdrawing group (NO_2) had markedly reduced affinity (K_i >1000 nM). No significant difference was observed in binding between bromo and iodo derivatives. On the basis of the encouraging data obtained for the iodinated derivatives **8** (K_i = 34.5 nM) and **10** (K_i = 6.6 nM), these two ligands were chosen for radio-labeling and further biological evaluations.

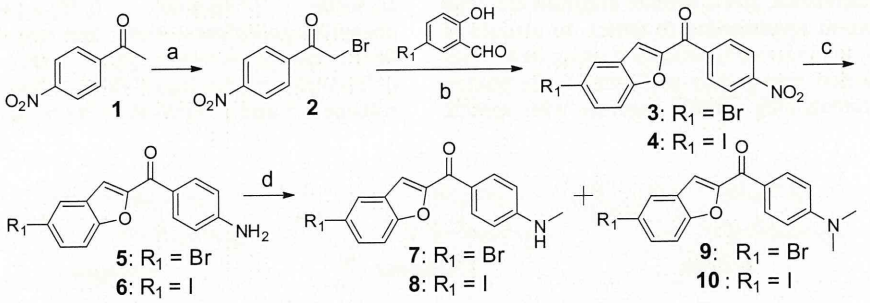

Scheme 1. Reagents and conditions: (a) Br_2, Et_2O, 0 °C, rt; (b) acetone, K_2CO_3, rt; (c) $SnCl_2$, EtOH, HCl, reflux; (d) acetone, CH_3I, K_2CO_3.

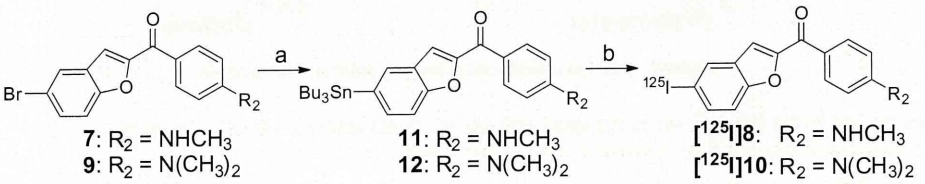

Scheme 2. Reagents and conditions: (a) $(Bu_3Sn)_2$,$(PPh_3)_4Pd$, dioxane, Et_3N, reflux; (b) [^{125}I]NaI, HCl (1M), H_2O_2 (3%), rt.

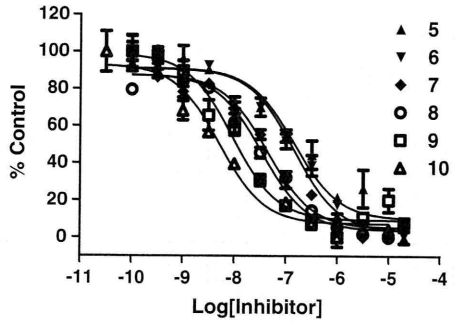

Figure 3. Inhibition curves of compounds **5–10** for $A\beta_{1-42}$ aggregates V.S [^{125}I]IMPY.

Table 1
Inhibition constants (K_i, nM) of compounds for the binding of [^{125}I]IMPY to $A\beta_{1-42}$ aggregates

Compound	R_1	R_2	K_i[a] (nM)
3	Br	NO_2	>1000
4	I	NO_2	>1000
5	Br	NH_2	156.6 ± 23.3
6	I	NH_2	133.2 ± 10.4
7	Br	$NHCH_3$	44.9 ± 9.7
8	I	$NHCH_3$	34.5 ± 7.3
9	Br	$N(CH_3)_2$	8.8 ± 3.9
10	I	$N(CH_3)_2$	6.6 ± 1.0
IMPY	—	—	10.5 ± 1.0

[a] Values are the mean for three independent experiments.

2.3. Radiolabeling

The desired radioiodinated ligands [^{125}I]**8** and [^{125}I]**10** were successfully prepared from the corresponding tributyltin precursors through standard iododestannylaltion reactions, using sodium [^{125}I]iodide, hydrogen peroxide, and hydrochloric acid (Scheme 2). The overall radiochemical yield for [^{125}I]**8** and [^{125}I]**10** was 83.5% and 34.1%, respectively. The radiochemical identity of the ^{125}I-labeled ligands was confirmed by co-injection with nonradioactive compounds on HPLC profiles (Fig. 4). The radiochemical purity of the purified ligands was greater than 97% and all had high specific activity (no carrier added, approx. 2200 Ci/mmol).

2.4. Autoradiography in vitro using AD transgenic mouse brain sections

Autoradiography in vitro using sections of brain tissue from double transgenic mice was selected for characterizing the specific binding of these radioiodinated ligands to Aβ plaques. As shown in Figure 5, [^{125}I]**10** showed excellent binding to Aβ plaques in the brain sections with numerous signals in the cortex region and minimal background labeling (Fig. 5A). The same section was also stained with thioflavin-S, a dye commonly used for Aβ plaques, and the distribution of Aβ plaques was consistent with the results of autoradiography (Fig. 5B, red arrow). However, the *N*-methylamino ligand, [^{125}I]**8**, displayed less intense labeling (data not shown). This could be due to the lower affinity (K_i = 34.5 nM) of **8** than that of **10**. Therefore, we abandoned this *N*-methylamino-ligand and focused only on [^{125}I]**10**.

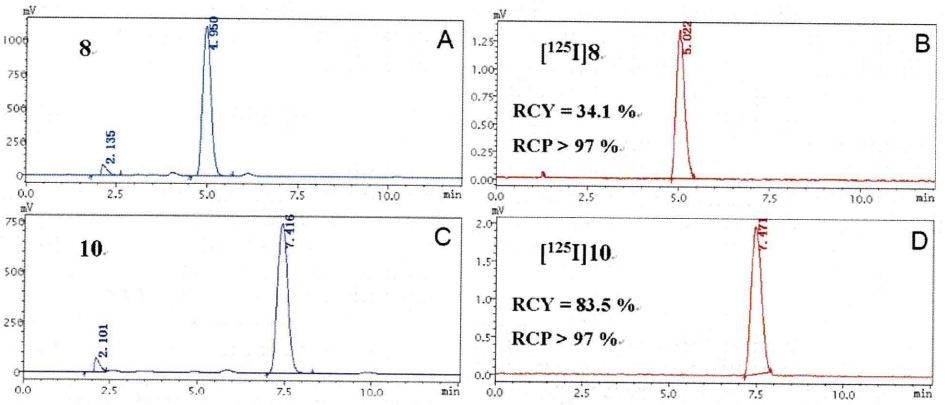

Figure 4. HPLC profiles of **8** (A), [^{125}I]**8** (B) and **10** (C), [^{125}I]**10** (D). HPLC conditions: Cosmosil C_{18} column (Nacalai Tesque, $5C_{18}$-AR-II, 4.6 mm × 150 mm), CH_3CN/H_2O = 75/25, 1 mL/min, UV, 254 nM, **8**tR (UV) = 4.95 min, [^{125}I]**8**tR (RI) = 5.02 min and **10**tR (UV) = 7.42 min, [^{125}I]**10**tR (RI) = 7.47 min.

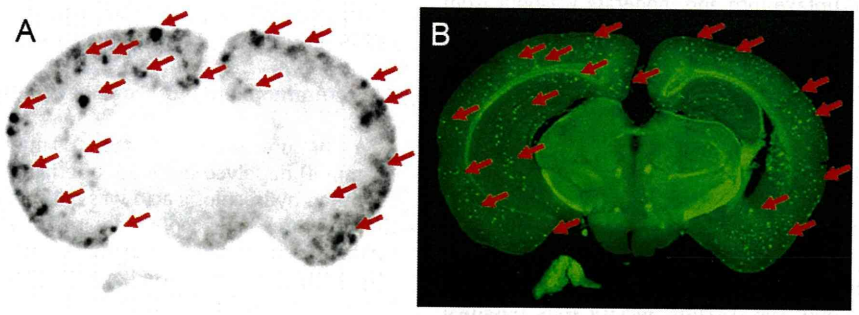

Figure 5. In vitro autoradiography of [^{125}I]**10** in a brain section of AD model mice (C57, APP/PS1, 12 months) (A). The same section was also stained with thioflavin-S (B) and the distribution of Aβ plaques was consistent with the results of autoradiography (red arrows).

Table 2
Biodistribution in normal ddy mice after i.v. injection of [^{125}I]**10** and the lipophilicity (log *D*) of the ligand[a]

Organ	[^{125}I]**10** log *D* = 4.40 ± 0.30				
	2 min	15 min	30 min	60 min	120 min
Blood	2.56 ± 0.25	1.16 ± 0.19	1.07 ± 0.29	0.82 ± 0.13	0.63 ± 0.15
Brain	3.53 ± 0.24	2.38 ± 0.39	1.51 ± 0.25	0.87 ± 0.15	0.41 ± 0.11
Heart	7.01 ± 0.86	1.45 ± 0.23	1.15 ± 0.41	0.74 ± 0.26	0.49 ± 0.08
Liver	16.19 ± 2.28	11.00 ± 1.13	6.70 ± 1.42	5.09 ± 0.74	3.59 ± 0.53
Spleen	2.75 ± 0.71	1.59 ± 0.32	0.94 ± 0.34	0.66 ± 0.02	0.43 ± 0.09
Lung	7.34 ± 1.90	2.20 ± 0.31	1.61 ± 0.38	0.94 ± 0.13	0.79 ± 0.20
Kidney	10.26 ± 1.52	3.84 ± 0.86	4.28 ± 1.18	1.90 ± 0.09	1.64 ± 0.39
Stomach[b]	0.95 ± 0.05	1.54 ± 0.61	2.60 ± 0.31	3.10 ± 0.51	3.76 ± 0.29
Intestine	3.14 ± 0.18	11.77 ± 2.12	21.81 ± 3.08	20.88 ± 3.90	25.19 ± 3.69
Thyriod[b]	0.02 ± 0.01	0.05 ± 0.02	0.18 ± 0.07	0.46 ± 0.09	0.80 ± 0.37

[a] Expressed as % injected dose per gram. Average for five mice ± standard deviation.
[b] Expressed as % injected dose per organ.

2.5. Biodistribution experiments with normal mice

To evaluate the kinetic properties of [^{125}I]**10** in vivo, biodistribution experiments were performed in normal mice. As shown in Table 2, the *N,N*-dimethylamino ligand [^{125}I]**10** displayed good penetration of the blood–brain barrier with an initial brain uptake of 3.53% ID/g at 2 min post-injection. Since there are no Aβ plaques in normal mice, the level of radioactivity in the brain decreased rapidly, being 0.87% ID/g at 60 min. In addition, the blood background during the experiment was low compared with the brain uptake, which is better for reducing nonspecific binding. The ratio $brain_{2\ min}/brain_{30\ min}$ is considered an important index for selecting tracers with appropriate kinetics in vivo. [^{125}I]**10** showed a $brain_{2\ min}/brain_{30\ min}$ ratio of 2.34. Compared with radioiodinated *N,N*-dimethylamino chalcones (4.16) and aurones (7.27) reported previously,[17,21] [^{125}I]**10** had superior initial brain uptake (3.53% ID/g) but the ratio of $brain_{2\ min}/brain_{30\ min}$ (2.34) was lower, which may be due to its high lipophilicity (log *D* = 4.40 ± 0.30). As can be expected from the relatively high log *D* value, [^{125}I]**10** was excreted predominantly by the hepatobiliary system. The hepatobiliar excretion to the intestines was also rather fast, and radioactivity was observed to accumulate within the intestine at later time points (25.19% ID/g at 120 min p.i.). Consistently, the accumulation of radioactivity in the thyroid increased gradually with time, suggesting that [^{125}I]**10** was not stable to in vivo deiodination.

3. Conclusions

In conclusion, we successfully synthesized and evaluated a series of benzofuran-2-yl(phenyl)methanone derivatives by Rap–Stoermer condensation as probes for Aβ plaques. The *N, N*-dimethylamino and *N*-methylamino ligands displayed high affinity for Aβ aggregates in a binding assay in vitro. When labeled with ^{125}I, the *N,N*-dimethylamino derivative **10** showed specific labeling of Aβ plaques in the brain sections of AD model mice. In addition, [^{125}I]**10** displayed good uptake into and moderate washout from the brain after injections in normal mice. Taken together, the present results suggest the novel benzofuran-2-yl(phenyl)methanone derivatives to be useful probes for detecting Aβ plaques in the AD brain.

4. Experimental section

4.1. General information

All the chemicals used were commercial products employed without further purification. The ^{1}H NMR spectra were obtained at 400 MHz on JEOL JNM-AL400 NMR spectrometers in $CDCl_3$ solutions at room temperature with TMS as an internal standard. Chemical shifts are reported as δ values relative to the internal TMS. Coupling constants are reported in Hertz. Multiplicity is defined by s (singlet), d (doublet), t (triplet), and m (multiplet). Mass spectra were acquired with Shimadzu GC–MS-QP2010 Plus (APCI). HPLC was performed with a Shimadzu system (a LC-10AT pump with a SPD-10A UV detector, λ = 254 nM) using a column of Cosmosil C_{18} (Nacalai Tesque, $5C_{18}$-AR-II, 4.6 mm × 150 mm) and acetonitrile/water = 75/25 as the mobile phase at a flow rate of 1.0 mL/min. All key compounds were proven by this method to show ⩾95% purity (see supplementary data).

4.2. 2-Bromo-1-(4-nitrophenyl)ethanone (2)

To a solution of **1** (1.65 g, 10 mmol) in dry ethylether (150 mL) was added Br_2 (1.60 g, 10 mmol) dropwise in an ice bath. The reaction mixture was stirred at room temperature for 2 h. Evaporation of the solvent afforded 2.29 g of **2** as a white crystal (94%). ^{1}H NMR (400 MHz, $CDCl_3$) δ 8.35 (d, *J* = 9.1 Hz, 2H), 8.15 (d, *J* = 9.1 Hz, 2H), 4.47 (s, 2H).

4.3. (5-Bromobenzofuran-2-yl)(4-nitrophenyl)methanone (3)

A mixture of **2** (488 mg, 2 mmol), 5-bromosalicylaldehyde (402 mg, 2 mmol), and K_2CO_3 (276 mg, 2 mmol) in acetone (10 mL) was stirred at room temperature for 8 h, and the reaction mixture was washed with water to give **3** in 84% yield (580 mg). ^{1}H NMR (400 MHz, $CDCl_3$) δ 8.41 (d, *J* = 8.9 Hz, 2H), 8.23 (d, *J* = 8.9 Hz, 2H), 7.91 (d, *J* = 1.9 Hz, 1H), 7.65 (dd, *J* = 8.8, 2.0 Hz, 1H), 7.56 (d, *J* = 0.9 Hz, 1H), 7.54 (dd, *J* = 8.8, 0.4 Hz, 1H). HRMS (EI): *m/z* calcd for $C_{15}H_8BrNO_4$ 344.9629; found 344.9636.

4.4. (5-Iodobenzofuran-2-yl)(4-nitrophenyl)methanone (4)

The reaction described for **3** was used, and **4** was obtained in a yield of 87%. ^{1}H NMR (400 MHz, $CDCl_3$) δ 8.41 (d, *J* = 8.7 Hz, 2H), 8.22 (d, *J* = 8.6 Hz, 2H), 8.12 (d, *J* = 1.7 Hz, 1H), 7.81 (dd, *J* = 8.8, 1.7 Hz, 1H), 7.54 (d, *J* = 0.8 Hz, 1H), 7.43 (dd, *J* = 8.8, 0.8 Hz, 1H). HRMS (EI): *m/z* calcd for $C_{15}H_8INO_4$ 392.9491; found 392.9498.

4.5. (4-Aminophenyl)(5-bromobenzofuran-2-yl)methanone (5)

A mixture of **3** (344 mg, 1.0 mmol) and $SnCl_2$ (380 mg, 2.0 mmol) dissolved in 50 mL of ethanol containing 2 mL of concentrated hydrochloric acid was stirred under reflux for 2 h. After the mixture had cooled to room temperature, 2 M NaOH (100 mL) was added and extracted with ethyl acetate (100 mL). The organic layer was dried over Na_2SO_4. The filtrate was concentrated to give 283 mg of **5** (90%). ^{1}H NMR (400 MHz, $CDCl_3$) δ 8.01 (dd, *J* = 8.7, 1.0 Hz, 2H), 7.90–7.81 (m, 1H), 7.55 (ddt, *J* = 4.1, 2.2, 1.1 Hz, 1H), 7.50 (d, *J* = 8.8 Hz, 1H), 7.42 (s, 1H), 6.73 (dd, *J* = 8.7,

0.9 Hz, 2H), 4.25 (s, 2H). HRMS (EI): *m/z* calcd for $C_{15}H_{10}BrNO_2$ 314.9889; found 314.9894.

4.6. (4-Aminophenyl)(5-iodobenzofuran-2-yl)methanone (6)

The reaction described for **5** was used, and **6** was obtained in a yield of 81%. ^{1}H NMR (400 MHz, CD_3OD) δ 8.15 (d, J = 1.5 Hz, 1H), 7.94 (d, J = 8.8 Hz, 2H), 7.77 (dd, J = 8.7, 1.8 Hz, 1H), 7.51 (d, J = 0.9 Hz, 1H), 7.46 (d, J = 8.8 Hz, 1H), 6.72 (d, J = 8.8 Hz, 2H), 4.85 (s, 2H). HRMS (EI): *m/z* calcd for $C_{15}H_{10}INO_2$ 362.9752; found 362.9756.

4.7. (5-Bromobenzofuran-2-yl)(4-(methylamino)phenyl)methanone (7)

To a solution of **5** (315 mg, 1 mmol) in acetone (15 mL) was added CH_3I (0.18 mL, 3 mmol) and anhydrous K_2CO_3 (138 mg, 1 mmol). The reaction mixture was stirred at room temperature for 12 h and poured into water. The mixture was extracted with ethyl acetate. The organic layers were combined and dried over Na_2SO_4. Evaporation of the solvent afforded a residue, which was purified by silica gel chromatography to give 108 mg of **7** (33%). ^{1}H NMR (400 MHz, $CDCl_3$) δ 8.06 (d, J = 9.0 Hz, 2H), 7.85 (dd, J = 1.9, 0.5 Hz, 1H), 7.55 (dd, J = 8.8, 1.9 Hz, 1H), 7.52–7.48 (m, 1H), 7.41 (d, J = 0.9 Hz, 1H), 6.65 (d, J = 8.9 Hz, 2H), 4.49 (s, 1H), 2.95 (s, 3H). HRMS (EI): *m/z* calcd for $C_{16}H_{12}BrNO_2$ 329.0042; found 329.0051.

4.8. (5-Iodobenzofuran-2-yl)(4-(methylamino)phenyl)methanone (8)

The reaction described for **7** was used, and **8** was obtained in a yield of 41%. ^{1}H NMR (400 MHz, $CDCl_3$) δ 8.03 (d, J = 1.8 Hz, 1H), 8.03 (d, J = 8.9 Hz, 2H), 7.70 (dd, J = 8.8, 1.2 Hz, 1H), 7.44–7.29 (m, 2H), 6.63 (d, J = 8.9 Hz, 2H), 2.92 (s, 3H). HRMS (EI): *m/z* calcd for $C_{16}H_{12}INO_2$ 376.9904; found 376.9913.

4.9. (5-Bromobenzofuran-2-yl)(4-(dimethylamino)phenyl)methanone (9)

The reaction described for **7** was used, and **9** was obtained in a yield of 26%.^{1}H NMR (400 MHz, $CDCl_3$) δ 8.10 (d, J = 9.2 Hz, 2H), 7.85 (d, J = 1.7 Hz, 1H), 7.54 (dd, J = 8.8, 1.7 Hz, 1H), 7.50 (d, J = 8.8 Hz, 1H), 7.41 (d, J = 0.8 Hz, 1H), 6.74 (d, J = 9.1 Hz, 2H), 3.11 (s, 6H). HRMS (EI): *m/z* calcd for $C_{17}H_{14}BrNO_2$ 343.0200; found 343.0207.

4.10. (4-(Dimethylamino)phenyl)(5-iodobenzofuran-2-yl)methanone (10)

The reaction described for **7** was used, and **10** was obtained in a yield of 37%. ^{1}H NMR (400 MHz, $CDCl_3$) δ 8.10 (d, J = 9.0 Hz, 2H), 8.05 (s, 1H), 7.71 (d, J = 8.7 Hz, 1H), 7.40 (d, J = 8.7 Hz, 1H), 7.39 (s, 1H), 6.74 (d, J = 9.1 Hz, 2H), 3.11 (s, 6H). HRMS (EI): *m/z* calcd for $C_{17}H_{14}INO_2$ 391.0061; found 391.0069.

4.11. (4-(Methylamino)phenyl)(5-(tributylstannyl)benzofuran-2-yl)methanone (11)

A mixture of **7** (165 mg, 0.5 mmol), $(Bu_3Sn)_2$ (0.5 mL), and $(Ph_3P)_4Pd$ (60 mg, 0.04 mmol) in a mixed solvent (10 mL, 4:1 dioxane/Et_3N) was stirred under reflux for 10 h. The solvent was removed, and the residue was purified by silica gel chromatography to give 48 mg of **11** (18%). ^{1}H NMR (400 MHz, $CDCl_3$) δ 8.07 (d, J = 8.6 Hz, 2H), 7.79 (s, 1H), 7.61 (d, J = 8.1 Hz, 1H), 7.52 (d, J = 8.1 Hz, 1H), 7.47 (s, 1H), 6.64 (d, J = 8.6 Hz, 2H), 4.36 (s, 1H), 2.95 (s, 3H), 1.82–0.57 (m, 27H). MS (APCI): *m/z* calcd for $C_{28}H_{39}NO_2Sn$ 541.20; found 542.30 ($M+H^+$).

4.12. (4-(Dimethylamino)phenyl)(5-(tributylstannyl)benzofuran-2-yl)methanone (12)

The reaction described for **11** was used, and **12** was obtained in a yield of 29%. ^{1}H NMR (400 MHz, $CDCl_3$) δ 8.11 (d, J = 8.8 Hz, 2H), 7.80 (s, 1H), 7.61 (d, J = 8.1 Hz, 1H), 7.52 (d, J = 8.1 Hz, 1H), 7.47 (s, 1H), 6.74 (d, J = 8.9 Hz, 2H), 3.10 (s, 6H), 1.69–0.76 (m, 27H). MS (APCI): *m/z* calcd for $C_{29}H_{41}NO_2Sn$ 555.22; found 556.30 ($M+H^+$).

4.13. Radiolabeling

The radioiodinated ligands [^{125}I]**8** and [^{125}I]**10** were prepared from the corresponding tributyltin precursor through an iododestannylation reaction according to a procedure described previously with some modifications.[17] Briefly, 50 μL of H_2O_2 (3%) was added to a mixture of a tributyltin derivative (0.1 mg/100 μL in ethanol), 200 μCi of sodium [^{125}I]iodide (specific activity 2200 Ci/mmol), and 100 μL of 1 M HCl in a sealed vial. The reaction was allowed to proceed at room temperature for 15 min and then quenched with the addition of 50 μL of a saturated $NaHSO_3$ solution. The reaction mixture was extracted with ethyl acetate (3 × 1 mL) after neutralization with 10 mg of sodium bicarbonate. The combined extracts were evaporated dry. The residues were dissolved in 100 μL of EtOH and purified by HPLC using a $5C_{18}$-AR-II analytical column (4.6 × 150 mm), CH_3CN/H_2O = 3/1, at a flow rate of 1.0 mL/min. The desired fractions containing the product were evaporated dry and redissolved in 100% ethanol. Finally, the radiochemical identity of [^{125}I]**8** and [^{125}I]**10** was verified by co-injection with nonradioactive compounds by HPLC. The final product was stored at −20 °C until use for autoradiography and biodistribution experiments.

4.14. Binding assay in vitro using $A\beta_{1-42}$ aggregates

Inhibition experiments were carried out in 12 × 75 mm borosilicate glass tubes according to a procedure described previously with some modifications.[22] One hundred microliters of aggregated Aβ fibrils (60 nM in the final assay mixture) was added to a mixture containing 100 μL of radioligand ([^{125}I]IMPY) of the appropriate concentration, 10 μL of inhibitor (10^{-5}–10^{-10} M in ethanol), and 790 μL of PBS (0.2 M, pH 7.4) in a final volume of 1 mL. Nonspecific binding was defined in the presence of 1 μM IMPY. The mixture was incubated for 2 h at 37 °C with constant shaking, then the bound and free radioactivity were separated by vacuum filtration through borosilicate glass fiber filters (Whatman GF/B) using a cell harvester (Brandel, M-24 Gaithersburg, MD, USA). Filters containing the bound ^{125}I ligand were measured for radioactivity in a γ-counter (WALLAC/Wizard 1470, USA) with 70% counting efficiency. Under the assay conditions, the specifically bound fraction accounted for about 10% of all the radioactivity. The half maximal inhibitory concentration (IC_{50}) was determined using GRAPHPAD PRISM 4.0, the inhibition constant (K_i) was calculated using the Cheng-Prusoff equation: $K_i = IC_{50}/(1 + [L]/K_d)$.[23]

4.15. Autoradiography in vitro using AD transgenic mouse brain sections

Paraffin-embedded brain sections of AD model mice (C57, APP/PS1, 12 months) were used for autoradiography. The sections were deparaffinized with 2 × 20 min washes in xylene; 2 × 5 min washes in 100% ethanol; a 5 min wash in 90% ethanol/H_2O; a 5 min wash in 80% ethanol/H_2O; a 5 min wash in 60% ethanol/H_2O and a 10 min wash in running tap water, and then incubated

in PBS (0.2 M, pH 7.4) for 30 min. The sections were incubated with radiotracers (5 μCi/100 μL) for 1 h at room temperature. They were then washed with 40% ethanol for 3 min, and rinsed with water for 30 s. After drying, the ^{125}I-labeled sections were exposed to a Fuji Film imaging plate overnight. The in vitro autoradiographic images were obtained using a BAS5000 scanner system (Fuji Film). The presence and location of plaques in the sections were confirmed by fluorescent staining with thioflavin-S (1 μM).

4.16. Biodistribution experiments with normal mice

The biodistribution experiments were performed in normal ddY mice (female, 5 weeks) and approved by the animal care committee of Kyoto University. A saline solution (100 μL, 5% EtOH) containing [^{125}I]**10** (0.9 μCi) was injected directly into the tail vein. The mice were sacrificed at various time points post-injection. The organs of interest were removed and weighed, and the radioactivity was measured with an automatic γ-counter. The percentage dose per gram of wet tissue was calculated by a comparison of the tissue counts to suitably diluted aliquots of the injected material.

4.17. Determination of the partition co-efficient

The partition co-efficient of the radioligand was determined as described previously but with some modifications.[17] Radioligand (10 μCi) was added to premixed suspensions containing 3 g of *n*-octanol and 3 g of PBS (0.05 M, pH 7.4) in a test tube. The test tube was vortexed for 3 min at room temperature, and centrifuged for 5 min at 3000 rpm. Two weighted samples from the *n*-octanol (50 μL) and buffer (800 μL) layers were measured. The partition co-efficient was expressed as the logarithm of the ratio of the counts per gram from *n*-octanol versus PBS. Samples from the *n*-octanol layer were repartitioned until consistent partitions of co-efficient values were obtained. The measurement was done in triplicate and repeated three times.

Acknowledgments

This study was supported by the Funding Program for Next Generation World-Leading Researchers, and a Grant-in-aid for Young Scientists (A) and Exploratory Research from the Ministry of Education, Culture, Sports, Science and Technology, Japan. This study was also supported by the China Scholarship Council (CSC).

Supplementary data

Supplementary data associated with this article can be found, in the online version, at doi:10.1016/j.bmc.2011.04.049.

References and notes

1. Selkoe, D. J. *JAMA-J. Am. Med. Assoc.* **2000**, *283*, 1615.
2. Selkoe, D. J. *Physiol. Rev.* **2001**, *81*, 741.
3. Hardy, J. A.; Selkoe, D. J. *Science* **2002**, *297*, 353.
4. Mathis, C. A.; Wang, Y.; Klunk, W. E. *Curr. Pharm. Des.* **2004**, *10*, 1469.
5. Cai, L. S.; Innis, R. B.; Pike, V. W. *Curr. Med. Chem.* **2007**, *14*, 19.
6. Mathis, C. A.; Wang, Y.; Holt, D. P.; Huang, G. F.; Debnath, M. L.; Klunk, W. E. *J. Med. Chem.* **2003**, *46*, 2740.
7. Klunk, W. E.; Engler, H.; Nordberg, A.; Wang, Y.; Blomqvist, G.; Holt, D. P.; Bergstrom, M.; Savitcheva, I.; Huang, G. F.; Estrada, S.; Ausen, B.; Debnath, M. L.; Barletta, J.; Price, J. C.; Sandell, J.; Lopresti, B. J.; Wall, A.; Koivisto, P.; Antoni, G.; Mathis, C. A.; Langstrom, B. *Ann. Neurol.* **2004**, *55*, 306.
8. Koole, M.; Lewis, D.; Buckley, C.; Nelissen, N.; Vandenbulcke, M.; Brooks, D. J.; Vandenberghe, R.; Laere, K. V. *J. Nucl. Med.* **2009**, *50*, 818.
9. Rowe, C. C.; Ackerman, U.; Browne, W.; Mulligan, R.; Pike, K. L.; O'Keefe, G.; Tochon-Danguy, H.; Chan, G.; Berlangieri, S. U.; Jones, G.; Dickinson-Rowe, K. L.; Kung, H. F.; Zhang, W.; Kung, M. P.; Skovronsky, D.; Dyrks, T.; Holl, G.; Krause, S.; Friebe, M.; Lehman, L.; Lindemann, S.; Dinkelborg, L. M.; Masters, C. L.; Villemagne, V. L. *Lancet Neurol.* **2008**, *7*, 129.
10. Zhang, W.; Oya, S.; Kung, M. P.; Hou, C.; Maier, D. L.; Kung, H. F. *Nucl. Med. Biol.* **2005**, *32*, 799.
11. Zhang, W.; Kung, M.-P.; Oya, S.; Hou, C.; Kung, H. F. *Nucl. Med. Biol.* **2007**, *34*, 89.
12. Choi, S. R.; Golding, G.; Zhuang, Z. P.; Zhang, W.; Lim, N.; Hefti, F.; Benedum, T. E.; Kilbourn, M. R.; Skovronsky, D.; Kung, H. F. *J. Nucl. Med.* **2009**, *50*, 1887.
13. Kung, H. F.; Choi, S. R.; Qu, W. C.; Zhang, W.; Skovronsky, D. *J. Med. Chem.* **2010**, *53*, 933.
14. Kung, M. P.; Hou, C.; Zhuang, Z. P.; Zhang, B.; Skovronsky, D.; Trojanowski, J. Q.; Lee, V. M.; Kung, H. F. *Brain Res.* **2002**, *956*, 202.
15. Zhuang, Z. P.; Kung, M. P.; Wilson, A.; Lee, C. W.; Plossl, K.; Hou, C.; Holtzman, D. M.; Kung, H. F. *J. Med. Chem.* **2003**, *46*, 237.
16. Newberg, A. B.; Wintering, N. A.; Plossl, K.; Hochold, J.; Stabin, M. G.; Watson, M.; Skovronsky, D.; Clark, C. M.; Kung, M. P.; Kung, H. F. *J. Nucl. Med.* **2006**, *47*, 748.
17. Ono, M.; Haratake, M.; Mori, H.; Nakayama, M. *Bioorg. Med. Chem.* **2007**, *15*, 6802.
18. Ono, M.; Hori, M.; Haratake, M.; Tomiyama, T.; Mori, H.; Nakayama, M. *Bioorg. Med. Chem.* **2007**, *15*, 6388.
19. Ono, M.; Watanabe, R.; Kawashima, H.; Cheng, Y.; Kimura, H.; Watanabe, H.; Haratake, M.; Saji, H.; Nakayama, M. *J. Med. Chem.* **2009**, *52*, 6394.
20. Ono, M.; Maya, Y.; Haratake, M.; Ito, K.; Mori, H.; Nakayama, M. *Biochem. Biophys. Res. Commun.* **2007**, *361*, 116.
21. Maya, Y.; Ono, M.; Watanabe, H.; Haratake, M.; Saji, H.; Nakayama, M. *Bioconjug. Chem.* **2009**, *20*, 95.
22. Zhuang, Z. P.; Kung, M. P.; Hou, C.; Skovronsky, D. M.; Gur, T. L.; Plossl, K.; Trojanowski, J. Q.; Lee, V. M. Y.; Kung, H. F. *J. Med. Chem.* **2001**, *44*, 1905.
23. Cheng, Y.; Prusoff, W. *Biochem. Pharmacol.* **1973**, *22*, 3099.

Hindawi Publishing Corporation
International Journal of Molecular Imaging
Volume 2011, Article ID 543267, 12 pages
doi:10.1155/2011/543267

Review Article

SPECT Imaging Agents for Detecting Cerebral β-Amyloid Plaques

Masahiro Ono and Hideo Saji

Graduate School of Pharmaceutical Sciences, Kyoto University, 46-29 Yoshida Shimoadachi-cho, Sakyo-ku, Kyoto 606-8501, Japan

Correspondence should be addressed to Masahiro Ono, ono@pharm.kyoto-u.ac.jp and Hideo Saji, hsaji@pharm.kyoto-u.ac.jp

Received 29 July 2010; Revised 6 November 2010; Accepted 24 January 2011

Academic Editor: Alexander Drzezga

The development of radiotracers for use *in vivo* to image β-amyloid (Aβ) plaques in cases of Alzheimer's disease (AD) is an important, active area of research. The presence of Aβ aggregates in the brain is generally accepted as a hallmark of AD. Since the only definitive diagnosis of AD is by postmortem staining of affected brain tissue, the development of techniques which enable one to image Aβ plaques *in vivo* has been strongly desired. Furthermore, the quantitative evaluation of Aβ plaques in the brain could facilitate evaluation of the efficacy of antiamyloid therapies currently under development. This paper reviews the current situation in the development of agents for SPECT-based imaging of Aβ plaques in Alzheimer's brains.

1. Introduction

Alzheimer's disease (AD) is an age-related, irreversible form of dementia characterized by memory loss, a progressive decline in intellectual ability, language impairment, and personality and behavioral changes that eventually interfere with daily life. The accumulation of β-amyloid (Aβ) aggregates (major protein aggregates of senile plaques) in the brain is considered one of the hallmarks of AD [1, 2]. Today, the clinical diagnosis of AD is primarily based on history and memory testing, which is often difficult and not accurate, as the early cognitive and behavioral symptoms of AD are difficult to distinguish from normal signs of aging. To facilitate the early diagnosis of this disease, there is an urgent need for the sensitive noninvasive detection of biomarkers for the pathophysiology. Toward achieving this goal, nuclear imaging techniques such as positron emission computed tomography (PET) and single photon emission computed tomography (SPECT) have been employed. Radionuclide-labeled agents targeting the Aβ plaques in the brain may greatly facilitate the diagnosis of AD and new antiamyloid therapies [3–7]. The differential diagnosis for AD includes a large number of other diseases such as vascular dementia, frontal temporal lobe dementia (FTLD) complex, and dementia with Lewy bodies (DLB) as well as rarer neurodegenerative diseases such as Creutzfeld-Jacob disease (CJD). Importantly, AD subjects will always have Aβ plaques, whereas Aβ is seen not at all or only sporadically in most of these other diseases. In each case, appropriate prognosis and treatment require accurate diagnostic assessment.

Developing Aβ imaging agents is currently an emerging field of research. The basic requirements for suitable Aβ imaging agents include (i) good penetration of the blood-brain barrier, (ii) selective binding to Aβ plaques, and (iii) clear and contrasting signals between plaques and nonplaques (Figure 1). Based on these requirements, several promising agents with the backbone structure of DDNP, thioflavin-T and Congo Red have been synthesized and evaluated for use *in vivo* as probes to image Aβ plaques in AD brain. Clinical trials in AD patients have been conducted with several PET imaging agents including [^{11}C]PIB [8–10], [^{11}C]SB-13 [6, 11], [^{11}C]BF-227 [12], [^{11}C]AZD2184 [13], [^{18}F]FDDNP [14–16], [^{18}F]BAY94-9172 [7, 17, 18], [^{18}F] AV-45 [19–21], and [^{18}F]GE-067 [22] (Figure 2), indicating the imaging of Aβ plaques in living brain tissue to be useful for the diagnosis of AD. The ^{11}C-labeled agents limit their use to on-site cyclotrons and sophisticated radiochemistry laboratories due to the short half-life (20 min) of ^{11}C. PET agents with the longer half-life (110 min) radioisotope ^{18}F have recently been developed and could increase the availability of Aβ imaging to all PET facilities, but still represents a minority of modern hospitals, as only a small fraction of hospitals have a PET scanner. Since SPECT is more valuable than PET in terms of routine diagnostic

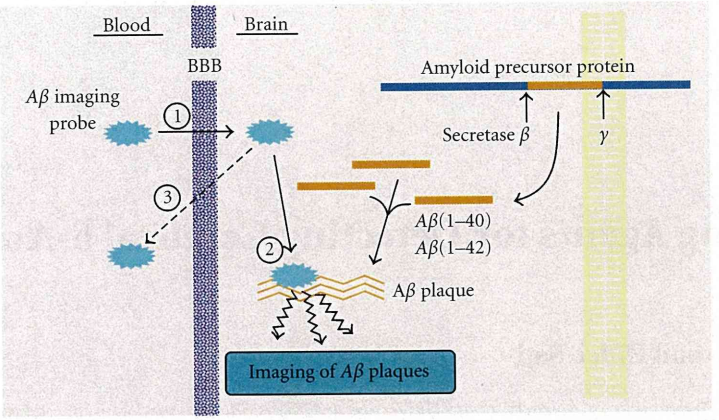

FIGURE 1: Strategy of *in vivo* imaging of cerebral Aβ plaques.

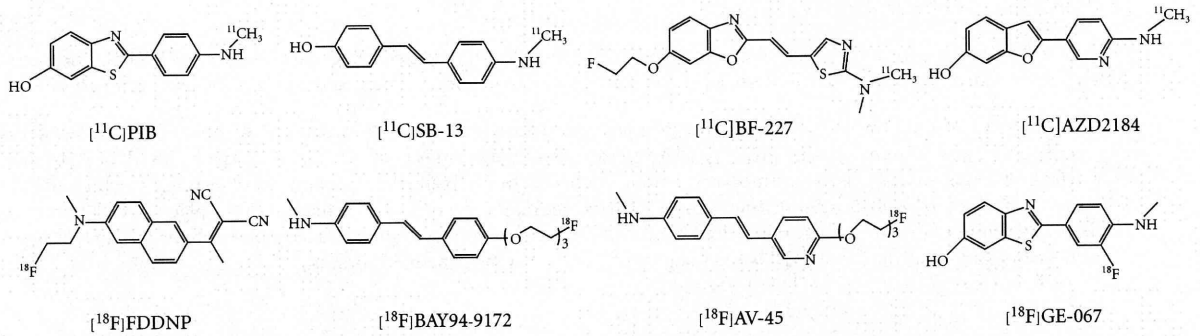

FIGURE 2: Chemical structure of PET imaging agents tested clinically.

use, the development of more useful Aβ imaging agents for SPECT has been a critical issue. However, progress in developing imaging agents targeting Aβ plaques is less advanced for SPECT than PET. In this review, we summarize the current situation in the development of probes for SPECT-based imaging of Aβ plaques in Alzheimer's brains.

2. Radioiodinated Probes for Imaging of Aβ Plaques

Many radioiodinated imaging agents derived from Congo Red or thioflavin-T have been developed. Compounds **1** [29], **2** [29], **3** [40], **4** [23], **5** [24], and **6** [25] (Figure 3) are thought to be derived from Congo Red. Although **1**, **2**, and **3** showed unfavorable pharmacokinetics *in vivo* such as low uptake into the brain and a slow washout, the radioactivity pharmacokinetics of **5** and **6** was much improved. Because thioflavin-T has a lower molecular weight than Congo Red, implying greater blood-brain penetration, a number of groups have worked to develop probes for SPECT derived from thioflavin-T including **7** (IMPY) [26–28], **8** (TZDM) [29], **9** (IBOX) [30], **10** (benzofuran derivatives) [31], and **11** (phenylindole derivatives) (Figure 4) [32].

Initially, Zhuang and coworkers prepared iodostrylbenzene derivatives based on the chemical structure of Congo Red, [^{125}I]IMSB (**1**) and [^{125}I]ISB (**2**). These ligands exhibited low brain uptake likely due to two ionizable carboxyl groups [29]. Thus, a small and neutral thioflavin-T analog, [^{125}I]TZDM (**8**), was prepared [29]. *In vitro* binding studies of these ligands, [^{125}I]ISB, [^{125}I]IMSB and [^{125}I]TZDM, showed excellent binding affinities with K_d values of 0.08, 0.13 and 0.06 nM for aggregates of Aβ(1–40) and 0.15, 0.73 and 0.14 nM for aggregates of Aβ(1–42), respectively. Interestingly, in a competitive-binding assay, different binding sites on Aβ(1–40) and Aβ(1–42) aggregates, which are mutually exclusive, were observed for Congo Red and thioflavin-T derivatives. Biodistribution experiments in normal mice after an i.v. injection showed that [^{125}I]TZDM exhibited good uptake and retention in the brain, much higher than [^{125}I]ISB and [^{125}I]IMSB. Preliminary experiments on the biodistribution of [^{125}I]TZDM in transgenic mice, engineered to produce excess Aβ plaques in the brain as an AD model, suggested labeling of Aβ aggregates *in vivo*. However, [^{125}I]TZDM is not ideal as an imaging agent *in vivo*, due to its labeling of white matter, which significantly increases the background

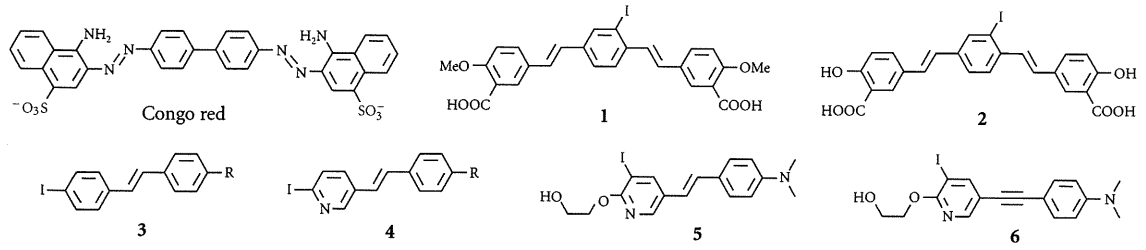

FIGURE 3: Chemical structure of SPECT imaging agents derived from Congo Red.

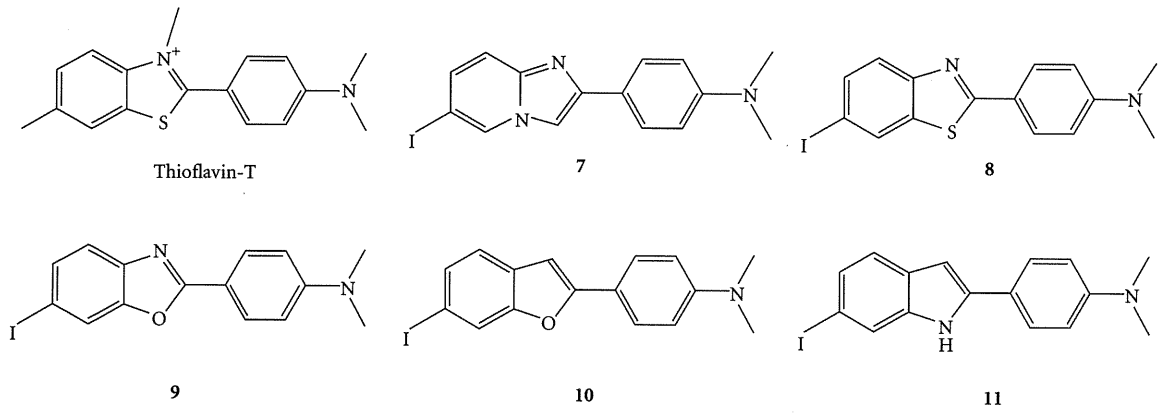

FIGURE 4: Chemical structure of SPECT imaging agents derived from thioflavin T.

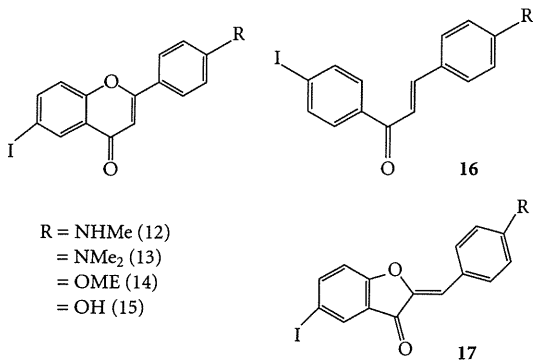

FIGURE 5: Chemical structure of SPECT imaging agents based on flavone (**12–15**), chalcone (**16**), and aurone (**17**).

activity. To improve the pharmacokinetics of uptake and retention, Kung et al. and others have prepared several compounds derived from thioflavin-T and studied features such as affinity for Aβ aggregates *in vitro* and biodistribution *in vivo*. Interestingly, the compounds with good binding to Aβ aggregates share a common structural feature: either an *N*-methylamino- or *N,N*-dimethylaminophenyl group at one end of the molecule. The structural feature required for binding to Aβ aggregates appears to be simple and unique.

[^{123}I]IMPY has been characterized as a potential agent for SPECT-based imaging of Aβ plaques. IMPY displayed selective labeling of Aβ plaques *ex vivo* in autoradiographic experiments using double-transgenic mice (PSAPP) as a model of AD [33]. Preliminary clinical data on [^{125}I]IMPY in normal and AD patients showed a distinct distribution pattern similar to that of [^{11}C]PIB [34, 35]. However, the signal-to-noise ratio for plaque labeling is not as high as that of [^{11}C]PIB. The low contrast may be due to the fast clearance from brain and plasma observed in AD and normal subjects. But the rapid metabolism and instability of [^{123}I]IMPY *in vivo* may have led to less than optimal signal-to-noise ratios for targeting Aβ plaques in the brain. Additional candidates are being explored for SPECT imaging of Aβ plaques in the brain.

Recently, the effects of polyhydroxyflavones on the formation, extension, and destabilization of Aβ aggregates have been studied *in vitro* [36]. These flavones dose-dependently inhibited the formation of Aβ aggregates, as well as destabilized preformed Aβ aggregates, indicating that they could interact directly with the aggregates. The findings in that report prompted us to use flavones as a core structure in the development of Aβ imaging agents. Furthermore, some recent studies have shown that electron-donating groups such as methylamino, dimethylamino, methoxy, and hydroxy groups play a critical role in the binding to Aβ aggregates. With these considerations in mind, we designed

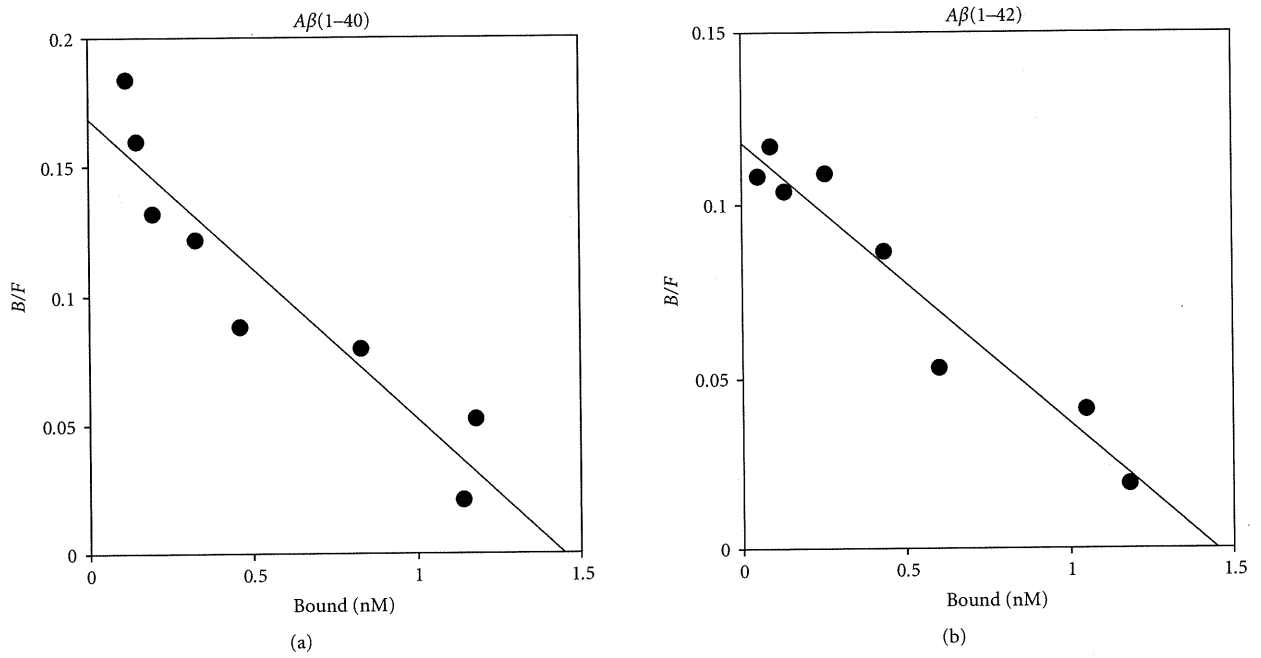

FIGURE 6: Scatchard plots of the binding of [^{125}I]**12** to aggregates of Aβ(1–40) (a) and Aβ(1–42) (b).

four radioiodinated flavones with a radioiodine at the 6-position and an electron-donating group at the 4′-position (Figure 5). Then we synthesized a series of flavone derivatives and evaluated their usefulness *in vivo* as SPECT Aβ imaging agents [37].

Experiments on the binding of [^{125}I]**12** to aggregates of Aβ(1–40) and Aβ(1–42) were carried out. Transformation of the saturation binding of [^{125}I]**12** to Scatchard plots gave linear plots, suggesting one binding site (Figure 6). [^{125}I]**12** showed excellent affinity for both Aβ(1–40) (K_d = 12.4 ± 2.3 nM) and Aβ(1–42) (K_d = 17.4 ± 5.7 nM) aggregates. The binding of nonradioactive flavone derivatives (compounds **12**, **13**, **14**, and **15**) was evaluated in experiments inhibiting [^{125}I]**12** from binding Aβ(1–40) and Aβ(1–42) aggregates. As shown in Table 1, all flavone derivatives competed well with [^{125}I]**12** (K_i = 13–77 nM). More interestingly, when thioflavin-T, and Congo Red gave high K_i values (>1000 nM) (Table 1), indicating little competition. This finding suggests that these flavones may have a binding site on Aβ aggregates different from that of thioflavin T and Congo Red, although additional studies regarding the selectivity of binding affinity for Aβ aggregates are required.

Since the *in vitro* binding assays demonstrated the high affinity of the flavone derivatives for Aβ(1–40) and Aβ(1–42) aggregates, compounds **12**, **13**, **14**, and **15** were investigated for their neuropathologic staining of Aβ plaques and NFTs in human AD brain sections (Figure 7). The compounds intensely stained Aβ plaques (Figures 7(a), 7(e), 7(i), and 7(m)), neuritic plaques (Figures 7(b), 7(f), 7(j), and 7(n)), and cerebrovascular amyloids (Figures 7(c), 7(g), 7(k), and 7(o)) with nearly the same pattern. However, as seen in Figures 7(a), 7(e), 7(i), and 7(m), these flavone compounds did not intensely stain the core region in so-called classic Aβ plaques, unlike the thioflavin-T and Congo Red derivatives previously reported as Aβ imaging probes, indicating that flavone derivatives may have somewhat distinct binding characteristics for amyloid fibrils. These flavone derivatives appear to stain not only neuritic Aβ plaques but also diffuse amyloid plaque deposits, which are known to be mainly composed of Aβ(1−42) [38] and to be the initial pathologic change in AD [39]. Thus flavone derivatives with high affinity for Aβ(1–42)-positive diffuse plaques may be more useful for presymptomatic detection of AD. Furthermore, **12**, **13**, **14**, and **15** also showed high affinity for NFTs in AD brain sections (Figures 7(d), 7(h), 7(l), and 7(p)). These findings suggest that these flavone derivatives can bind amyloid fibrils and NFTs without the backbone structure of thioflavin-T or Congo Red and that quantitative evaluation of their cerebral

TABLE 1: Inhibition constants (K_i, nM)[a] of compounds for the binding of ligands to aggregates of Aβ(1–40) and Aβ(1–42).

Compound	Aβ(1–40)	Aβ(1–42)
12	22.6 ± 3.4	30.0 ± 3.4
13	13.2 ± 0.2	15.6 ± 2.4
14	29.0 ± 3.2	38.3 ± 8.1
15	72.5 ± 8.2	77.2 ± 9.2
Thioflavin T	>1000	>1000
Congo Red	>1000	>1000

[a]Values are the mean ± standard error of the mean for 6 independent experiments.

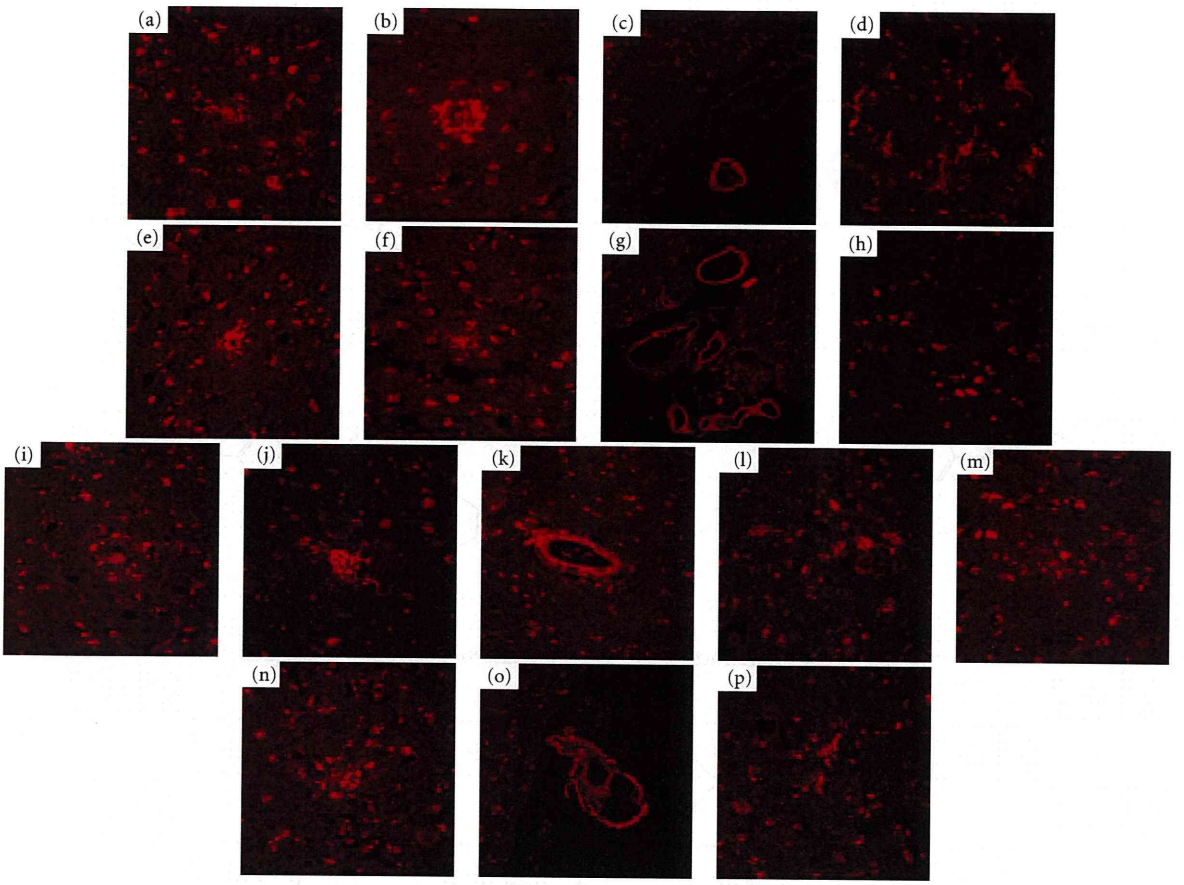

FIGURE 7: Neuropathological staining of compounds **12** (a)–(d), **13** (e)–(h), **14** (i)–(l), and **15** (m)–(p) on 5 μm AD brain sections from the temporal cortex. (a) Aβ plaques (a), (e), (i), and (m) are clearly stained with **12**, **13**, **14**, and **15** (×40 magnification). Clear staining of neuritic plaques (b), (f), (j), and (n) and cerebrovascular amyloid (c), (g), (k), and (o) was also obtained. Many NFTs (d), (h), (l), and (p) are intensely stained with **12**, **13**, **14**, and **15** (×40 magnification).

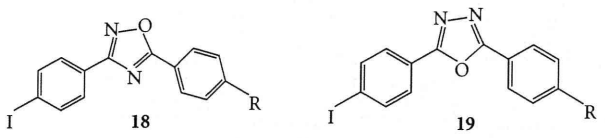

FIGURE 8: Chemical structure of diphenyl oxadiazoles.

localization may provide useful information on Aβ and tau pathology.

Four radioiodinated flavone ligands ([^{125}I]**12**, [^{125}I]**13**, [^{125}I]**14**, and [^{125}I]**15**) were evaluated for their biodistribution *in vivo* in normal mice. Previous studies suggest that the optimal lipophilicity range for brain entry is observed for compounds with log *P*-values between 1 and 3 [5]. All four ligands displayed optimal lipophilicity as reflected by log *P*-values of 1.94, 2.69, 2.41, and 1.92, respectively. As expected, these ligands exhibited high uptake ranging from 3.2% to 4.1% ID/g brain at 2 min postinjection, a level sufficient for imaging in the brain (Table 2). In addition, they displayed good clearance from the normal brain: 1.2, 1.0, 0.17, and 0.08% ID/g at 60 min postinjection for [^{125}I]**12**, [^{125}I]**13**, [^{125}I]**14**, and [^{125}I]**15**, respectively. Radioiodinated amyloid imaging agents such as [^{125}I]*m*-I-stilbene (**3**) [40], [^{125}I]TZDM (**8**) [29], [^{125}I]IBOX (**9**) [30], and [^{125}I]benzofuran (**10**) [31], and [^{125}I]phenylindole (**11**) [32] reported previously showed good uptake, but a relatively slow washout from the normal brain. A low washout rate leads to high background activity and prevents the visualization of Aβ plaques in the AD brain. Appropriate properties *in vivo* (higher uptake and faster washout from the normal brain) make radioiodinated flavones useful candidates for SPECT tracers for Aβ imaging.

On the basis of this success in the development of SPECT imaging agents, to search for more useful candidates for Aβ imaging probes, we have designed a chemical modification of the flavone structure, and selected the chalcone and aurone structure as a novel core for Aβ imaging probes (Figure 5) [41, 42]. Chalcone and aurone are categorized as flavonoids containing a flavone. We newly designed and synthesized novel chalcone and aurone derivatives, and evaluated the

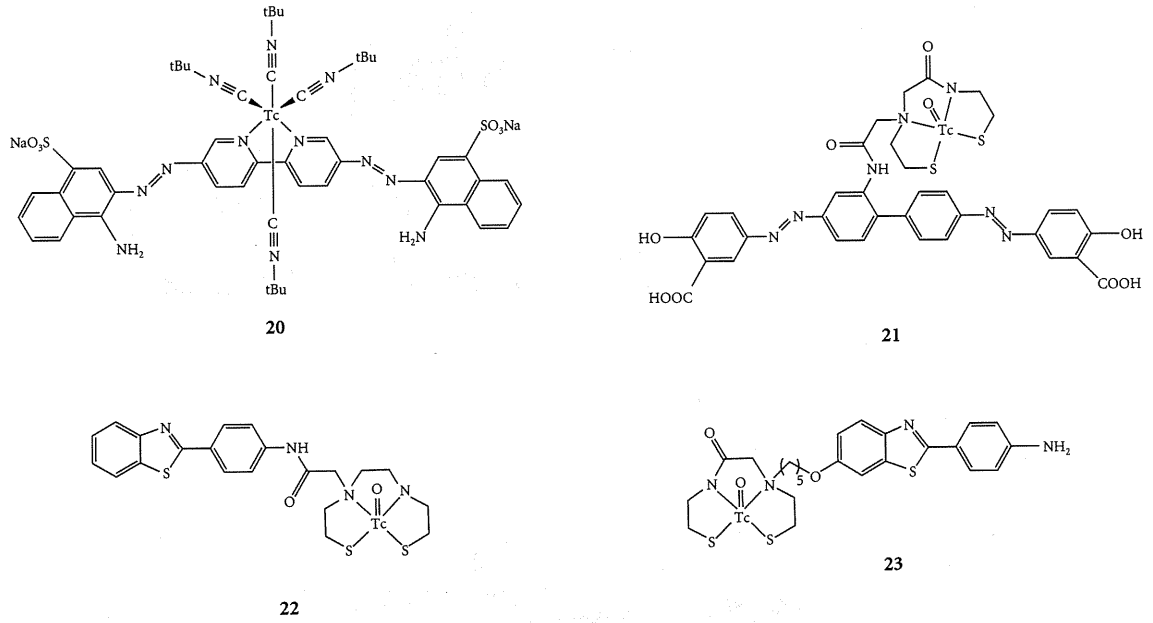

FIGURE 9: Chemical structure of ^{99m}Tc complexes for imaging of Aβ plaques.

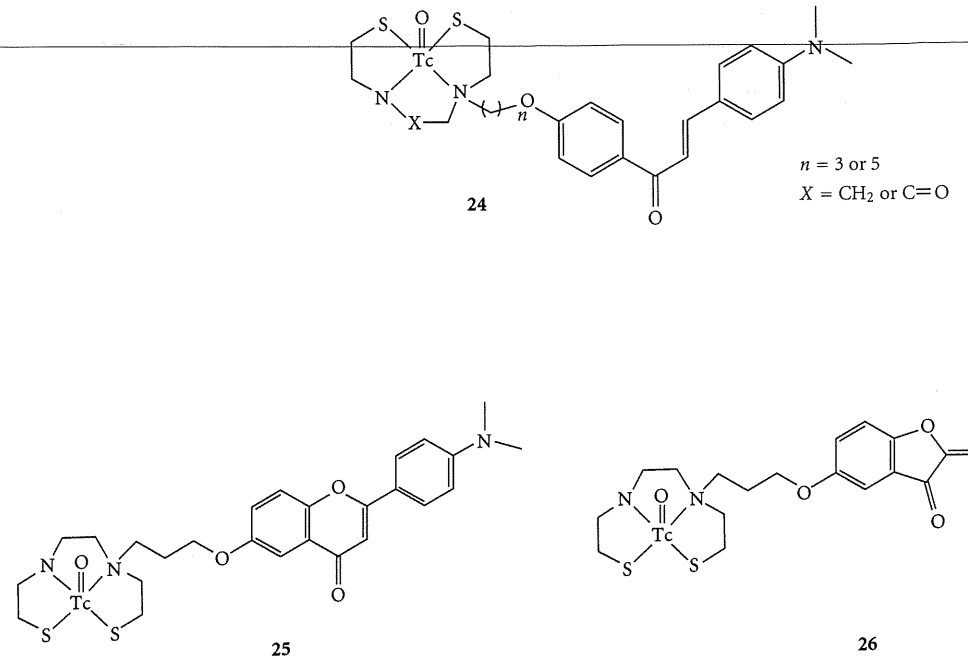

FIGURE 10: Chemical structure of ^{99m}Tc complexes based on chalcone (**24**), flavone (**25**), and aurone (**26**) for imaging of Aβ plaques.

effect of their structure–activity relationships on binding to Aβ aggregates and biodistribution *in vivo* using a compound with high affinity [42–45]. Currently, SPECT imaging agents based on chalcone and aurone are optimized.

Most of the Aβ imaging probes reported previously have two aromatic rings. Among them, 1,4-diphenyltriazole and 2,5-diphenylthiophene derivatives have triazole and thiophene between two benzene rings, respectively, and it has been shown that they have high-binding affinity for binding to Aβ aggregates despite the kinds of substituted groups [46, 47]. In an attempt to further develop novel ligands for the imaging of Aβ plaques in AD, we designed a series of 3,5-diphenyl-1,2,4-oxadiazole (**18**) [48, 49] and 2,4-diphenyl-1,3,5-oxadiazole (**19**) [49] derivatives (Figure 8). Although

Table 2: Biodistribution of radioactivity after intravenous injection of [^{125}I]**12**, [^{125}I]**13**, [^{125}I]**14**, and [^{125}I] **15** in normal mice[a]

Tissue	Time after injection (min)			
	2	10	30	60
		[^{125}I]**12**		
Blood	1.89 (0.28)	1.39 (0.10)	1.34 (0.07)	1.50 (0.09)
Liver	16.28 (0.90)	25.28 (0.31)	18.61 (1.81)	15.14 (0.89)
Kidney	8.13 (1.28)	5.21 (0.44)	3.85 (0.33)	3.05 (0.25)
Intestine	3.10 (0.61)	7.91 (1.05)	12.84 (1.18)	21.48 (3.17)
Spleen	2.57 (1.54)	2.31 (0.01)	1.76 (0.23)	1.52 (0.29)
Heart	4.87 (0.66)	2.66 (0.12)	1.67 (0.14)	1.28 (0.12)
Stomach[b]	0.78 (0.02)	0.87 (0.22)	1.44 (0.69)	1.80 (0.84)
Brain	4.12 (0.15)	3.68 (0.18)	1.84 (0.12)	1.19 (0.04)
		[^{125}I]**13**		
Blood	1.87 (0.18)	1.07 (0.08)	1.20 (0.15)	1.15 (0.16)
Liver	15.41 (0.98)	21.85 (2.14)	15.71 (0.96)	12.40 (2.38)
Kidney	8.33 (1.47)	4.31 (0.28)	3.40 (0.31)	2.32 (0.45)
Intestine	2.24 (0.24)	6.56 (0.83)	12.97 (1.15)	18.64 (2.05)
Spleen	2.72 (0.20)	1.92 (0.33)	1.58 (0.31)	1.18 (0.17)
Heart	5.63 (0.80)	2.47 (0.14)	1.69 (0.06)	1.07 (0.17)
Stomach[b]	0.73 (0.17)	0.63 (0.16)	1.17 (0.40)	1.06 (0.27)
Brain	3.22 (0.15)	3.61 (0.60)	1.89 (0.21)	0.99 (0.10)
		[^{125}I]**14**		
Blood	1.87 (0.21)	1.19 (0.17)	0.40 (0.01)	0.23 (0.09)
Liver	8.96 (1.48)	9.01 (0.97)	3.75 (0.47)	1.88 (0.61)
Kidney	7.99 (1.08)	6.30 (1.02)	4.51 (1.59)	1.46 (1.12)
Intestine	3.52 (0.29)	14.39 (0.80)	22.51 (1.11)	30.05 (3.61)
Spleen	2.70 (0.08)	1.38 (0.37)	0.55 (0.30)	3.67 (5.89)
Heart	4.98 (0.41)	2.25 (0.40)	0.84 (0.14)	0.47 (0.22)
Stomach[b]	0.68 (0.06)	0.45 (0.18)	0.55 (0.33)	0.31 (0.07)
Brain	4.00 (0.18)	2.36 (0.33)	0.51 (0.07)	0.17 (0.05)
		[^{125}I]**15**		
Blood	2.77 (0.43)	1.58 (0.18)	0.66 (0.03)	0.20 (0.02)
Liver	9.77 (1.89)	8.24 (0.50)	6.80 (0.86)	4.78 (1.09)
Kidney	14.79 (2.59)	15.11 (2.00)	6.45 (0.84)	1.66 (0.62)
Intestine	3.12 (0.37)	11.26 (0.63)	22.01 (1.34)	27.28 (0.48)
Spleen	3.92 (1.18)	1.55 (0.15)	0.56 (0.13)	0.17 (0.06)
Heart	5.51 (0.71)	1.60 (0.18)	0.53 (0.04)	0.12 (0.02)
Stomach[b]	0.89 (0.09)	0.59 (0.16)	1.56 (0.50)	0.81 (0.36)
Brain	3.31 (0.32)	1.90 (0.07)	0.52 (0.03)	0.08 (0.02)

[a]Expressed as % injected dose per gram. Each value represents the mean ± S.D. for 3–5 animals at each interval. [b]Expressed as % injected dose per organ.

the diphenyloxadiazole pharmacophore with high-binding affinity for Aβ aggregates may be useful as a backbone structure to develop novel Aβ imaging agents, additional modifications are necessary to improve the uptake and rapid clearance of nonspecifically bound radiotracers.

Many factors such as molecular size, ionic charge, and lipophilicity affect the brain uptake of compounds. Since lipophilicity of the compounds generally increases by introduction of iodine, the large higher lipophilicity of the radioiodinated compounds may constitute one reason for the low brain uptake. In the future, introduction of hydrophilic substituted groups into the amyloid-binding scaffolds will be required to develop more promising radioiodinated tracers with in favorable *in vivo* pharmacokinetics.

3. ^{99m}Tc Complexes for Imaging of Aβ Plaques

^{99m}Tc ($T_{1/2}$ = 6.01 h, 141 keV) has become the most commonly used radionuclide in diagnostics for SPECT, because it is readily produced by an ^{99}Mo/^{99m}Tc generator, the medium gamma-ray energy it emits is suitable for detection, and its physical half-life is compatible with the biological localization and residence time required for imaging. Its ready availability, essentially 24 h a day, and easiness

Table 3: Biodistribution of radioactivity after injection of ^{99m}Tc-labeled benzofuran derivatives in normal mice[a].

Organ	Time after injection (min)			
	2	10	30	60
		^{99m}Tc-BAT-BF (**27**)		
Blood	4.40 (0.27)	1.96 (0.06)	1.93 (0.26)	2.15 (0.91)
Liver	21.94 (5.94)	20.87 (1.28)	19.65 (1.31)	15.09 (3.83)
Kidney	10.28 (1.76)	7.90 (0.40)	4.27 (0.18)	2.70 (0.57)
Intestine[b]	1.45 (0.18)	3.68 (0.52)	7.42 (1.62)	9.02 (1.93)
Spleen	5.20 (1.01)	3.09 (0.23)	1.69 (0.21)	1.16 (0.14)
Lung	26.70 (2.27)	6.48 (1.33)	3.51 (0.64)	2.36 (0.48)
Stomach[b]	1.33 (0.57)	1.90 (0.43)	4.09 (1.37)	4.17 (1.92)
Pancreas	4.14 (0.77)	4.57 (0.24)	2.98 (0.38)	1.42 (0.15)
Heart	17.60 (2.60)	8.29 (0.97)	3.28 (1.35)	1.51 (0.25)
Brain	1.34 (0.12)	1.37 (0.18)	0.94 (0.20)	0.56 (0.07)
		^{99m}Tc-MAMA-BF (**28**)		
Blood	4.13 (0.42)	1.78 (0.25)	2.15 (0.12)	2.24 (0.24)
Liver	20.17 (3.81)	21.62 (2.62)	23.32 (1.59)	20.16 (2.13)
Kidney	7.37 (1.06)	8.09 (1.16)	5.11 (0.29)	3.28 (0.45)
Intestine[b]	0.95 (0.22)	2.13 (0.19)	4.75 (0.93)	5.73 (0.66)
Spleen	4.48 (0.56)	3.69 (0.34)	3.49 (0.61)	2.59 (0.65)
Lung	24.04 (5.17)	7.59 (2.13)	4.24 (0.35)	3.54 (1.26)
Stomach[b]	0.73 (0.21)	2.35 (0.58)	4.94 (0.57)	2.81 (0.51)
Pancreas	2.70 (0.47)	4.00 (1.28)	5.48 (0.61)	3.76 (0.36)
Heart	12.28 (2.20)	10.48 (1.79)	5.05 (0.90)	2.16 (0.34)
Brain	0.74 (0.15)	0.99 (0.22)	1.23 (0.09)	0.89 (0.08)

[a]Each value represents the mean (SD) for 5 mice. Expressed as % injected dose per gram. [b]Expressed as % injected dose per organ.

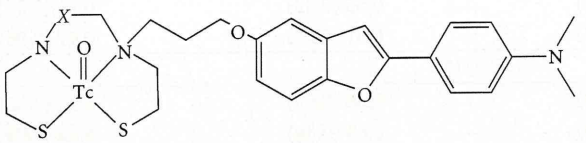

27: $X = CH_2$
28: $X = CO$

Figure 11: Chemical structure of ^{99m}Tc complexes based on the benzofuran scaffold for imaging of Aβ plaques.

of use make it the radionuclide of choice. New ^{99m}Tc-labeled imaging agents will provide simple, convenient, and widespread SPECT-based methods for detecting and eventually quantifying Aβ plaques in living brain tissue.

Han and co-workers described a positively charged ^{99}Tc-complex of Congo red (**20**) which binds to Aβ aggregates *in vitro* [50]. The basic structure of this complex is the Congo red backbone in which the biphenyl moiety is replaced by a bipyridyl moiety capable of complexing Tc in the presence of *tert*-butylisonitrile as a coligand. Although these Tc complexes showed high affinity for Aβ aggregates in vitro, they have not been tested *in vivo*. Dezutter and co-workers reported a ^{99m}Tc-labeled conjugate of Congo Red with a monoamide-monoaminedithiol (MAMA) chelating ligand [51]. However, brain uptake of this ^{99m}Tc-labeled Congo Red

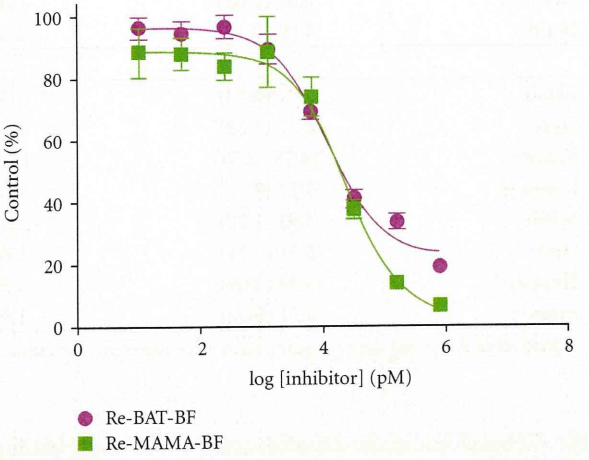

Figure 12: Inhibition curves of Re-BAT-BF and Re-MAMA-BF for the binding of [^{125}I]IMPY to Aβ(1–42) aggregates.

derivative (**21**) was minimal, probably because of its large size and ionized character at physiological pH. Serdons and co-workers reported the synthesis of a neutral ^{99m}Tc-labeled derivative of thioflavin-T (**22**), namely a benzothiazole derivative conjugated with a bisamine-bisthiol (BAT) ligand, and its biological characterization [52]. It was demonstrated

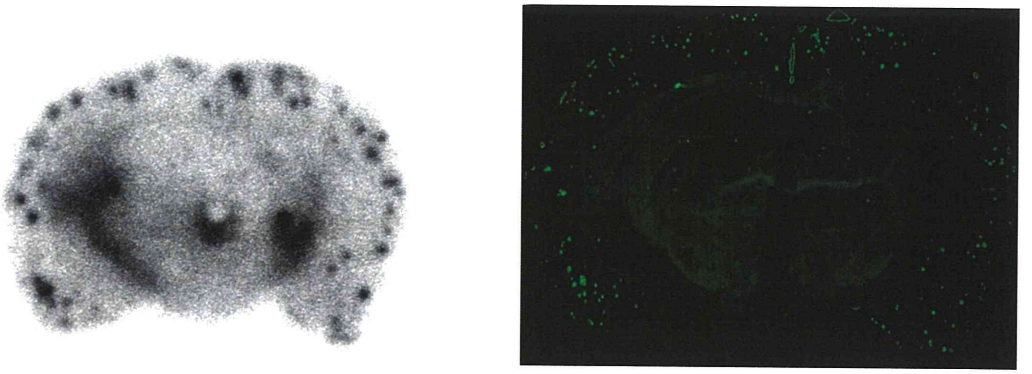

(a) (b)

FIGURE 13: Autoradiography of ^{99m}Tc-BAT-BF (**27**) in sections from Tg2576 mouse brain (a). Labeled plaques were confirmed by the staining of the adjacent sections with thioflavin S (b).

that the ^{99m}Tc-labeled thioflavin-T derivative binds *in vitro* to Aβ plaques. Despite its high lipophilicity and neutral character, the ^{99m}Tc complex did not cross the blood-brain barrier to a sufficient degree and thus is not useful for the detection of AD *in vivo*. Recently, Chen et al. reported that the ^{99m}Tc-labeled thioflavin T using MAMA as a chelation ligand (**23**) demonstrated the binding to Aβ aggregates in sections of brain tissue from transgenic mice and AD patients [53]. In addition, **23** can penetrate the blood-brain barrier with high initial brain uptake and moderate washout. These results are encouraging for further exploration of their derivatives as imaging agents for Aβ plaques in the brain.

As described above, several ^{99m}Tc-labeled imaging probes have been developed (Figure 9) [50–55], but no clinical study of them has been reported. While these ^{99m}Tc complexes showed high affinity for Aβ aggregates or Aβ plaques *in vitro*, they suffered the same unfavorable *in vivo* pharmacokinetics in normal mice, that is, a slow washout. Therefore, to make them promising probes for imaging Aβ plaques in the brain, additional molecular modifications to improve their pharmacokinetics *in vivo* are required.

Recently, we have developed several ^{99m}Tc complexes based on flavone, chalcone, aurone, and benzofuran derivatives with monoamine-monoamide dithiol (MAMA) and bis-amino-bis-thiol (BAT) as chelation ligands (Figures 10 and 11). MAMA and BAT were selected taking into consideration the permeability of the blood-brain barrier, because they form an electrically neutral complex with ^{99m}Tc [56]. We then evaluated their biological potential as probes by testing their affinity for Aβ aggregates and Aβ plaques in sections of brain tissue from Tg2576 mice and their uptake in and clearance from the brain in biodistribution experiments using normal mice.

Initially, four ^{99m}Tc-labeled chalcone derivatives and their corresponding rhenium analogues were tested as potential probes for imaging Aβ plaques (Figure 10) [57]. The chalcones showed higher affinity for Aβ(1–42) aggregates than did ^{99m}Tc complexes and, in sections of brain tissue from an animal model of AD, the four Re-chalcones intensely stained Aβ plaques. In biodistribution experiments using normal mice, ^{99m}Tc-BAT-chalcone (**24**) displayed high uptake in the brain (1.48%ID/g) at 2 min after injection. The radioactivity washed out from the brain rapidly (0.17%ID/g at 60 min), a highly desirable feature for an imaging agent. Although potential existence of *cis*- and *anti*-isomers was expected, one single isomer was isolated in the preparation of **24**, **25**, and **26**. The chemical identities of **24**, **25**, and **26** were confirmed by NMR and MS, but their absolute configurations have not yet been determined by X-ray crystallography.

As for ^{99m}Tc complexes based on benzofuran, we evaluated binding affinity using Re-BAT-BF and Re-MAMA-BF, analogs of ^{99m}Tc-BAT-BF (**27**) and ^{99m}Tc-MAMA-BF (**28**), respectively. Both ligands inhibited the binding of [^{125}I]IMPY to Aβ(1–42) aggregates in a dose-dependent manner, indicating an affinity for Aβ aggregates (Figure 12). Their K_i values were 11.5 and 24.4 nM, respectively, suggesting that Re-BAT-BF displayed higher affinity than Re-MAMA-BF. Next, the affinity of ^{99m}Tc-BAT-BF (**27**) for Aβ plaques was investigated *in vitro* using sections of Tg2576 mouse brain (Figure 13). Furthermore, the radioactivity of ^{99m}Tc-BAT-BF (**27**) corresponded with the areas of staining with thioflavin S, a dye commonly used for Aβ plaques. In contrast, normal mouse brain displayed no detectable accumulation of ^{99m}Tc-BAT-BF (**27**). The results suggest that ^{99m}Tc-BAT-BF (**27**) binds to Aβ plaques in the mouse brain in addition to synthetic Aβ aggregates.

The biodistribution of ^{99m}Tc-BAT-BF (**27**) and ^{99m}Tc-MAMA-BF (**28**) was examined in normal mice (Table 3). ^{99m}Tc-BAT-BF (**27**) showed greater uptake (1.34%ID/g) than ^{99m}Tc-MAMA-BF (**28**) (0.74%ID/g) at 2 min after injection. The uptake of ^{99m}Tc-BAT-BF (**27**) peaked at 10 min after injection, reaching 1.37%ID/g, sufficient uptake for Aβ imaging, and 60% of the radioactivity had been washed out from the brain by 60 min after injection. The uptake of ^{99m}Tc-MAMA-BF (**28**) peaked 30 min after the injection at 1.23%ID/g, and the washout from the brain was slower than that of ^{99m}Tc-BAT-BF (**27**) throughout the time course, which is unsuitable for imaging *in vivo*. The combination of good affinity for Aβ plaques, uptake,

and clearance makes ^{99m}Tc-BAT-BF (**27**) a promising probe for the detection of Aβ plaques in the brain. The results of the present study should provide useful information for the development of ^{99m}Tc-labeled probes for the imaging of Aβ plaques in the brain, although there are some difficulties associated with the large size of ^{99m}Tc complex in the molecular design of ^{99m}Tc-labeled Aβ imaging probes to enhance the penetration of blood-brain barrier.

4. Conclusion

Many PET probes targeting Aβ plaques in the brain have been tested clinically and demonstrated potential utility. Unfortunately, the short half-life (^{11}C; 20 min, ^{18}F; 110 min) of ^{11}C- or ^{18}F-labeled probes except ^{18}F-FDG limits their use at major academic PET facilities with on-site cyclotrons and sophisticated radiochemistry laboratories. On the other hand, many more hospitals have the capacity to perform SPECT. Aβ imaging probes labeled with SPECT isotopes especially the inexpensive and readily available ^{99m}Tc will have more widespread clinical applicability especially in developing countries that cannot afford expensive cyclotron and PET scanners. The development of novel ^{123}I- or ^{99m}Tc-labeled Aβ imaging probes may lead to simple and convenient SPECT imaging methods for detecting and eventually quantifying Aβ plaques in living brain tissue.

Acknowledgments

The results in this paper were partly obtained at Nagasaki University. They would like to express our sincere thanks to Professor Morio Nakayama for his helpful, continuous advice and support. The research reviewed in this paper was possible only through the dedication, enthusiasm, and creativity of all my coworkers, whose names are acknowledged in the publications from our laboratory cited here. These studies were supported by a Grant-in-aid for Young Scientists (A) and (B) from the Ministry of Education, Culture, Sports, Science and Technology, the Industrial Technology Research Grant Program from New Energy and Industrial Technology Development Organization (NEDO), the Program for Promotion of Fundamental Biomedical Innovation (NIBIO), and a Health Labour Sciences Research grant.

References

[1] D. J. Selkoe, "Alzheimer's disease: genes, proteins, and therapy," *Physiological Reviews*, vol. 81, no. 2, pp. 741–766, 2001.

[2] J. A. Hardy and G. A. Higgins, "Alzheimer's disease: the amyloid cascade hypothesis," *Science*, vol. 256, no. 5054, pp. 184–185, 1992.

[3] C. A. Mathis, Y. Wang, and W. E. Klunk, "Imaging β-amyloid plaques and neurofibrillary tangles in the aging human brain," *Current Pharmaceutical Design*, vol. 10, no. 13, pp. 1469–1492, 2004.

[4] A. Nordberg, "PET imaging of amyloid in Alzheimer's disease," *Lancet Neurology*, vol. 3, no. 9, pp. 519–527, 2004.

[5] M. Ono, "Development of positron-emission tomography/single-photon emission computed tomography imaging probes for in vivo detection of β-amyloid plaques in Alzheimer's brains," *Chemical and Pharmaceutical Bulletin*, vol. 57, no. 10, pp. 1029–1039, 2009.

[6] N. P. L. G. Verhoeff, A. A. Wilson, S. Takeshita et al., "In-vivo imaging of Alzheimer disease β-amyloid with [^{11}C]SB-13 PET," *American Journal of Geriatric Psychiatry*, vol. 12, no. 6, pp. 584–595, 2004.

[7] H. F. Kung, S. R. Choi, W. Qu, W. Zhang, and D. Skovronsky, "^{18}F stilbenes and styrylpyridines for PET imaging of Aβ plaques in Alzheimer's disease: a miniperspective," *Journal of Medicinal Chemistry*, vol. 53, no. 3, pp. 933–941, 2010.

[8] C. A. Mathis, Y. Wang, D. P. Holt, G. F. Huang, M. L. Debnath, and W. E. Klunk, "Synthesis and evaluation of ^{11}C-labeled 6-substituted 2-arylbenzothiazoles as amyloid imaging agents," *Journal of Medicinal Chemistry*, vol. 46, no. 13, pp. 2740–2754, 2003.

[9] W. E. Klunk, H. Engler, A. Nordberg et al., "Imaging brain amyloid in Alzheimer's disease with Pittsburgh Compound-B," *Annals of Neurology*, vol. 55, no. 3, pp. 306–319, 2004.

[10] N. M. Scheinin, S. Aalto, J. Koikkalainen et al., "Follow-up of [^{11}C]PIB uptake and brain volume in patients with alzheimer disease and controls," *Neurology*, vol. 73, no. 15, pp. 1186–1192, 2009.

[11] M. Ono, A. Wilson, J. Nobrega et al., "^{11}C-labeled stilbene derivatives as Aβ-aggregate-specific PET imaging agents for Alzheimer's disease," *Nuclear Medicine and Biology*, vol. 30, no. 6, pp. 565–571, 2003.

[12] Y. Kudo, N. Okamura, S. Furumoto et al., "2-(2-[2-dimethylaminothiazol-5-yl]ethenyl)-6-(2-[fluoro]ethoxy)benzoxazole: a novel PET agent for in vivo detection of dense amyloid plaques in Alzheimer's disease patients," *Journal of Nuclear Medicine*, vol. 48, no. 4, pp. 553–561, 2007.

[13] A. E. Johnson, F. Jeppsson, J. Sandell et al., "AZD2184: a radioligand for sensitive detection of β-amyloid deposits," *Journal of Neurochemistry*, vol. 108, no. 5, pp. 1177–1186, 2009.

[14] E. D. Agdeppa, V. Kepe, J. Liu et al., "Binding characteristics of radiofluorinated 6-dialkylamino-2-naphthylethylidene derivatives as positron emission tomography imaging probes for beta-amyloid plaques in Alzheimer's disease," *The Journal of Neuroscience*, vol. 21, no. 24, p. RC189, 2001.

[15] K. Shoghi-Jadid, G. W. Small, E. D. Agdeppa et al., "Localization of neurofibrillary tangles and beta-amyloid plaques in the brains of living patients with alzheimer disease," *American Journal of Geriatric Psychiatry*, vol. 10, no. 1, pp. 24–35, 2002.

[16] G. W. Small, V. Kepe, L. M. Ercoli et al., "PET of brain amyloid and tau in mild cognitive impairment," *New England Journal of Medicine*, vol. 355, no. 25, pp. 2652–2663, 2006.

[17] W. Zhang, S. Oya, M. P. Kung, C. Hou, D. L. Maier, and H. F. Kung, "F-18 Polyethyleneglycol stilbenes as PET imaging agents targeting Aβ aggregates in the brain," *Nuclear Medicine and Biology*, vol. 32, no. 8, pp. 799–809, 2005.

[18] C. C. Rowe, U. Ackerman, W. Browne et al., "Imaging of amyloid β in Alzheimer's disease with ^{18}F-BAY94-9172, a novel PET tracer: proof of mechanism," *The Lancet Neurology*, vol. 7, no. 2, pp. 129–135, 2008.

[19] W. Zhang, M. P. Kung, S. Oya, C. Hou, and H. F. Kung, "^{18}F-labeled styrylpyridines as PET agents for amyloid plaque imaging," *Nuclear Medicine and Biology*, vol. 34, no. 1, pp. 89–97, 2007.

[20] S. R. Choi, G. Golding, Z. Zhuang et al., "Preclinical properties of F-AV-45: a PET agent for Aβ plaques in the brain," *Journal of Nuclear Medicine*, vol. 50, no. 11, pp. 1887–1894, 2009.